1963

Annealing of radiation-induced defects in polycrystalline bismuth

Mattackal Kuruvilla Verghese
Iowa State University

ANNEALING OF RADIATION-INDUCED DEFECTS IN POLYCRYSTALLINE BISMUTH

by

Mattackal Kuruvilla Verghese

A Dissertation Submitted to the
Graduate Faculty in Partial Fulfillment of
The Requirements for the Degree of
DOCTOR OF PHILOSOPHY

Major Subject: Nuclear Engineering

Approved:

Signature was redacted for privacy.

In Charge of Major Work

Signature was redacted for privacy.

Head of Major Department

Signature was redacted for privacy.

Dean of Graduate College

Iowa State University
Of Science and Technology
Ames, Iowa

1963

I. INTRODUCTION

Shortly after the invention of nuclear chain reactors, Wigner (1) pointed out that energetic radiation might cause disorder in the structure and properties of materials. Further investigations in the later years proved conclusively that the defect structure introduced by irradiation in a material is indeed highly complex in its nature and that its effect on the properties of materials could be of great concern to nuclear and space technologists. Solid state scientists also have become involved in this field of research because of the wide scope of radiation damage studies in understanding the behavior of imperfections in crystals.

In spite of the extensive work done in this area, much of the basic mechanism of radiation damage still remains unknown as stated by Billington (2, p. 99):

> "...our ignorance about the behaviour of metals under irradiation far exceeds our knowledge in this field, particularly with regard to the basic theory of the radiation damage process "

One of the basic facts revealed through research in the recent years is that some of the defects introduced by radiation anneal out in many different ways depending on the type and distribution of defects, the temperature, the purity of the material used, the crystal structure and several other factors. Experimental studies of these annealing processes

have helped a great deal in testing the validity of many of the theoretical models that have been put forth to explain the mechanism of radiation damage.

The purpose of this thesis is to investigate a proposed annealing process that could be quite dominant in polycrystalline metals, to predict theoretically the nature of the annealing kinetics for this process and to check the theory with an experiment showing the validity of such an annealing process in polycrystalline bismuth.

The theoretical model presented in Section III is a fairly simple treatment of the problem. It is hoped that this thesis will be a guide for a more rigorous theoretical treatment. Section IV deals with the experimental investigation carried out on polycrystalline bismuth and the results obtained are analysed and presented in Section V.

II. REVIEW OF LITERATURE

Wigner's suggestion in the latter part of 1942, that energetic radiation would cause atomic displacements in solids, prompted an immediate program for theoretical and experimental investigation on the nature and magnitude of radiation effects in the materials of interest in reactor technology. Publication of these basic studies did not commence until 1946. Much of this early work was concerned with practical problems of radiation damage in the development of nuclear reactors. Most of this data, however, was published without a thorough knowledge of the radiation flux, the impurity concentrations in the material and in many cases without reference to even the temperature.

A. Methods of Investigation

The first formal theory on production of displacements was published by Bohr (3) in 1948. Seitz (4) investigated this theory further and outlined some basic theoretical results on displacements caused by fast massive particles. Soon after this, it was discovered that the defects caused by radiation are often inhomogeneously distributed in the material in the form of concentrated clusters involving several thousands of atoms. Two important models were

presented to explain the formation of these clusters. Brinkman (5, 6) proposed his displacement spike model which is of remarkable physical significance and accounts for the high degree of mixing that occurs in the spike. Seitz and Koehler (7) in their well-known review article presented the thermal spike model which at the present time is believed to be the more common mechanism of spike formation than the displacement spike theory. The latter is believed to be important only in heavy metals.

The problem of understanding the mechanism of radiation defect formation does not end with these theoretical models. Experimental physicists tried to observe these defects directly. However, since these defects are often only of atomic dimensions, the scope of direct observation in quantitative studies of radiation damage has been so far very limited. Almost all the experimental investigation in this field has been based on the fact that the presence of atomic defects alters many physical and mechanical properties of the solid, such as electrical and thermal conductivity, optical parameters, density, stored energy, critical shear stress, chemical kinetics and many others. The attempt has been to measure the change in one of these properties during irradiation of a solid and to try to determine the defect concentration by comparing the experimental result with the theoretical value of the additional change in the particular

property that is measured, due to the introduction of imperfections.

Because of the ease and precision possible in its measurement, electrical resistivity is the most commonly studied property, but theoretical estimation of the extra electrical resistivity caused by even simple point defects like the interstitials and vacancies can become quite involved and is complicated by the fact that it requires knowledge of the scattering potential associated with these imperfections. Dexter (8) approximated this with a shielded coulomb interaction and using the Born approximation he found that for copper, silver and gold, one atomic per cent of vacancies would add an extra resistivity of 0.4$\mu\Omega$-cm, and a similar calculation for interstitials showed 0.6$\mu\Omega$-cm/per cent interstitial. Using the negative Hartree potential and the free electron approximation, Jongenburger (9, 10, 11) made detailed estimates for vacancies and interstitials and obtained 1.3, 1.5, and 1.5$\mu\Omega$-cm/per cent vacancies in copper, silver and gold respectively and about 5$\mu\Omega$-cm/per cent interstitials in copper. Later Blatt (12) refined Jongenburger's calculation and estimated that in copper the extra resistivity due to one per cent vacancies or one per cent interstitials is 1.4$\mu\Omega$-cm. Overhauser and Gorman (13) reexamined the problem by considering in detail the effect of the elastic displacement of atoms near the imperfections

on the residual resistivity of copper. They noticed that the scattering from the strained region of an interstitial is an order of magnitude greater than that from the defect itself. Their final results are 10.5 $\mu\Omega$-cm/per cent interstitials and 1.5$\mu\Omega$-cm/per cent vacancies.

From the discrepancies in these theoretical values of the electrical resistivity due to point defects, it is clear that it is rather unreliable to interpret the experimental data based on the theoretical results available at the present time. This theoretical approach is valid only in the case of electron irradiation which produces the simplest defect structure.

A second method of studying the point defects and the atomic mechanisms responsible for their formation and motion is by carrying out thermal annealing of the metal subsequent to irradiation and by measuring the physical property changes during annealing. The rate and kinetics of motion of these defects are found to be very helpful in testing the existing theories of radiation effects. It should be emphasized that the annealing behavior of irradiated materials is quite complex. A great deal of work has been done in this area and a wide variety of interpretations have been put forth; however no single one of them has been found to be entirely satisfactory. All the important work in this direction that was done till 1957 is reviewed by Dienes and

Vineyard (14). This book presents a broad and integrated review of the basic experimental investigation of the nature and properties of the radiation induced defects and their annealing mechanisms. A source book for a summarized review, in particular of the important publications till 1961 is by Billington and Crawford (15). This book also lists about 200 references on the work done on many different materials such as metals and their alloys, semiconductors, dielectrics, organic materials, and reactor materials. An international symposium on radiation damage in solids and reactor materials was held by the International Atomic Energy Agency in May 1962 and the proceedings of this conference are published in three volumes. Volume I (16) contains review articles on the general theory of radiation damage and also articles on defect structure studies in pure metals. The article by Simmons, et al. (17) in this volume contains an interesting summary of all the facts that are well-checked by theory and by experiment and also all the items that are still unclear in the case of point defects in irradiated F.C.C. metals. He has considered all the possible geometrical configurations for single as well as small clusters of point defects. He also has summarized the different experimental techniques and the methods available for analysis of the results of these experiments.

B. Theory of Annealing

To understand annealing of radiation induced defects, it is necessary to know how mobile the defects are. A few attempts have been made to calculate the activation energies of formation and of motion of interstitials and vacancies in copper. Huntington (18) made this calculation for vacancies on the assumption that the s and p electrons behave as if free and the core electrons repel the other cores according to a Born-Mayer potential. He obtained the energy of formation of a vacancy in copper equal to 1.8 eV, which was later modified by Brooks (19) to 1.2 eV and its energy of formation was found to be 1.0 eV. For an interstitial in copper, Huntington (20) considered the two possible configurations, namely, the split-interstitial and the body-center interstitial and obtained an energy of formation equal to about five times that for a vacancy. He also found that the energy of interstitial motion in copper is only between 0.07 and 0.27 eV. However, because of the assumptions involved in his calculations, Huntington was not able to show which of the two interstitial configurations was the preferred one. Fumi (21) has attempted to extend Huntington's calculations to vacancies in gold. A fascinating theoretical study of the effects of focussing collisions by particles of a given energy and direction has been done by Gibson, et al. (22), using computer

techniques on a face-centered lattice consisting of 500 copper atoms. They set up the computational model assuming a surface energy and a Born-Mayer potential for the interaction between the atoms. In their results, the split-interstitial was found to be more stable than the body-center interstitial. The crowdion model was found highly unstable and Frenkel pairs were found stable only beyond a minimum separation.

Little theoretical work has been done for materials other than copper and gold. However, experimental investigation has revealed many interesting facts about annealing of radiation damage. The predominant mechanisms of annealing have been found to be different in different materials. A summary of facts that are known to be true at the present time for F.C.C. metals is given by Simmons, et al. (17). In the case of ionic crystals, annealing is now understood to be mainly by the motion of vacancies. However, their mobility again depends on the type of ion-vacancy. In semi-conductors, the annealing mechanism, according to Fletcher and Brown (23) can be described by simple diffusion theory. They divided up the annealing process into three stages; in the first stage the interstitial-vacancy pairs at nearest neighbor distance recombine. In the second stage, the pairs farther apart either come together or wander away from each other and in the third stage, the defects which wandered away in the second stage recombine with another defect of the opposite kind. Letaw

(24) suggested that thermal acceptor levels introduced in germanium anneal in two steps; first by formation of divacancies and then by large cluster formation and movement of these clusters to the surface. All the work that was done till 1959 on radiation effects in semiconductors was comprehensively reviewed and summarized at a conference held in Tennessee in May 1959 and the individual papers are published in the Journal of Applied Physics (25).

The various methods of analyzing the annealing data in order to obtain information about the motion of the defects are summarized in references (14) and (17). The most commonly used methods are by pulse annealing and by isothermal annealing as used by Overhauser (26). Both these methods have the disadvantage that if there are more than one annealing process taking place at a certain temperature, neither one of these methods provide a way to determine the individual activation energy of the two processes. In this respect, the method used by Glower (27) is particularly useful if the number of dominant annealing processes does not exceed two. The method of analysis is similar to that for a radioactive decay curve for a mixture of more than one isotope, because of the fact that annealing is also a rate process following the Arrhenius type equation of the form

$$\lambda = K e^{-\frac{E}{kT}} \qquad (1)$$

where λ = the rate of annealing

K = the rate constant

E = the activation energy

k = the Boltzmann constant

and T = the temperature of annealing

In spite of the erroneous exponential "stripping" of his experimental annealing curves for electrical resistivity, Glower was able to show that this original method of analysis was valid.

Except for reference (27), little work has been done on defect structure in bismuth crystals. From some electrical resistivity measurements made on bismuth at the Oak Ridge National Laboratory, it is known that the damage rate in bismuth is 2.22×10^{-1} ohm-cm/hour of irradiation at a fast neutron flux of 7×10^{11} neutrons/cm^2-sec and at 20°K (15, p. 115). At the same flux and temperature the damage rate in most of the other metals so far tested is only of the order of 10^{-6} ohm-cm/hour. This enormous increase in the electrical resistivity of bismuth due to neutron damage is because of the very low number of conduction electrons per atom available in bismuth. As pointed out by Dienes and Vineyard (14, p. 133), the activation energy for motion of defects in general can be expected to be correlated with the melting point which means that for bismuth, the activation energy of motion would be much less than for copper.

III. THEORETICAL INVESTIGATION

Annealing of radiation-induced defects in a solid is, in effect, a process of removal or inactivation of the defects to enable the solid to regain its normal structure and properties. Such a removal process is made possible only by the diffusion of these defects through the solid and hence if sinks or traps are introduced into this solid, it should have significant effect on the annealing kinetics of these defects. Therefore, it can be expected that in polycrystalline materials, the annealing kinetics will be quite different from that in single crystals because of the sinks available in the former in the form of grain boundaries. In this section an investigation of the effect of these grain boundaries on the annealing rate of radiation-induced defects in a polycrystalline metal will be presented.

The general principle used in the model to be discussed here is that point defects introduced in a material by irradiation diffuse through the crystal to the grain boundaries where they are trapped. These point defects can migrate to the boundary either as single defects or alternatively, they can form pairs of their own kind and then move to the boundary in pairs. Bartlett and Dienes (28) have considered the mobility of di-vacancies in copper and have shown that their activation energy for motion is about half of that for

a single vacancy. This result can be safely extended to the case of bismuth, since the lattice structure of bismuth is quite similar to that of copper. However, the question of whether the defects migrate as single defects or in pairs does not enter into the theoretical treatment of the problem to be presented here.

A theoretical relation between the annealing rate and the grain size can be derived by solving the diffusion equation. The assumptions used in this calculation are as follows:

1. The grain boundaries are perfect absorbers for point defects migrating to them.

2. The grain boundaries are practically unfillable sinks.

3. Annealing at the grain boundaries is much larger than at the surface of the specimens.

The first assumption is valid because of the fact that the strong forces in the boundary region will keep the defects bound to this region. It has been shown by Webb (29) that the second assumption is valid. A concentration of 10^{20} impurity atoms/cm^3 is required to saturate the grain boundaries. Since this is larger than the number of defect atoms in the irradiated specimens by several orders of magnitude, the grain boundaries do remain unsaturated. The last assumption is based on the relatively large area of grain

boundaries available in the samples used in the experiment compared to their surface area.

Based on these assumptions, each crystal grain can be treated as a region R containing all the radiation-induced defects (or clusters of defects) that migrate towards the surrounding grain boundary S (Figure 1) and are trapped at the boundary. Each grain is assumed to be spherical with the surface S being perfectly black to the defects that arrive at the surface. Because of complete absorption, the concentration of defects at these spherical boundaries will be zero at any time t.

It now becomes possible to treat the diffusion equation

$$D \nabla^2 C(r,t) = \frac{\partial C}{\partial t}(r,t) \qquad (2)$$

with the boundary conditions $C(r_o,t) = 0$ for a grain of equivalent radius r_o and $C(0,t)$ = a constant. Here, $C(r,t)$ is the concentration of defects at any point r and time t, and D is the diffusion coefficient in the region R.

By separation of variables and other conventional methods, a set of functions $\phi(r)$ may be found such that

$$\nabla^2 \phi(r) + \lambda^2 \phi(r) = 0 \qquad (3)$$

everywhere in the sphere and $\phi(0)$ is a finite constant and $\phi(r_o) = 0$

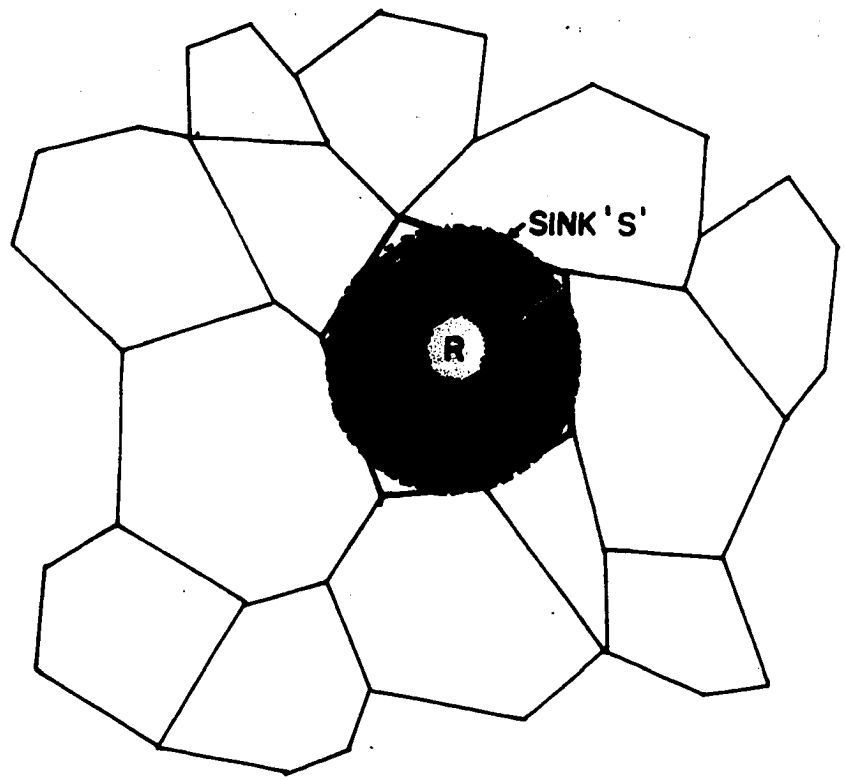

Figure 1. The region of diffusion R surrounded by the sink S

$$\frac{d^2 \phi(r)}{dr^2} + \frac{2}{r} \frac{d \phi(r)}{dr} + \lambda^2 \phi(r) = 0 \qquad (4)$$

Substituting $\phi = \frac{y}{r}$, Equation 3 reduces to

$$\frac{d^2 y}{dr^2} + \lambda^2 y = 0 \qquad (5)$$

which has the solution

$$y = A \cos \lambda r + B \sin \lambda r \qquad (6)$$

Therefore

$$\phi(r) = \frac{A \cos \lambda r}{r} \quad \frac{B \sin \lambda r}{r} \qquad (7)$$

Since $\phi(0)$ is finite, $A = 0$ and because $\phi(r_o) = 0$,

$$\frac{\sin \lambda r_o}{r_o} = 0 \qquad (8)$$

and

$$\lambda_n = \frac{n\pi}{r_o}, \quad n = 0,1,2,3,\ldots \qquad (9)$$

Therefore, the general solution to the diffusion problem can now be expressed as

$$C(r,t) = \sum_{n=1}^{\infty} \frac{B_n}{r} \sin\left(\frac{n\pi}{r_o} r\right) e^{-\frac{n^2\pi^2 D}{r_o^2} t} \qquad (10)$$

If t is large enough, the higher order terms of this

expression die out soon and

$$C(r,t) \sim \frac{B_1}{r} \operatorname{Sin} \left(\frac{\pi r}{r_o}\right) e^{-\frac{\pi^2 D}{r_o^2} t} \tag{11}$$

It follows from this result that the effective rate constant for annealing of the defects is

$$K = \frac{\pi^2 D}{r_o^2} \tag{12}$$

In other words, K is inversely proportional to r_o^2 or the rate constant of the annealing process is directly proportional to the number of grains per unit surface area. Therefore if the rate constant is determined experimentally for different grain sizes, it will be possible to check the validity of this theoretical result.

However, the problem might not be as simple as this treatment shows. Diffusion of defects to a sink may be strongly influenced by the stress field around the sink. This is known to be true in the case of an edge dislocation (30). Whether or not this is true for large angle grain boundaries is not known at the present time, because of the fact that there does not exist a valid mathematical model for large angle boundaries. According to McLean (31, p. 136), these boundaries do not interact like the dislocation grain boundaries with the point imperfections. In any case, large

angle boundaries have a finite width and the diffusion coefficient in the boundary region will be much larger than in the interior of the grain. Therefore the previous simple radial diffusion problem can be refined to diffusion taking place in a spherical region surrounded by a shell in which the diffusion coefficient D_2 is different from the diffusion coefficient D_1 in the core.

An analogous problem in heat conduction through composite spherical solids is solved by Carslaw (32). This calculation can be directly applied to our diffusion problem.

Consider a solid sphere of radius b of which an inner core $0 \leq r < a$ has a diffusion coefficient D_1 and a defect concentration $C_1(r,t)$ and in the outer shell, $a < r \leq b$ the corresponding quantities are D_2 and $C_2(r,t)$. Assume an initial concentration C and also as in the previous case, the concentration at the sink, $C_2(b,t) = 0$.

Substituting $u_1(r,t) = r\, C_1(r,t)$ and $u_2(r,t) = r\, C_2(r,t)$, the diffusion equations in the two regions reduce to

$$\frac{\partial u_1(r,t)}{\partial t} = D_1 \frac{\partial^2 u_1(r,t)}{\partial r^2}, \quad 0 \leq r < a, \; t > 0 \qquad (13)$$

and

$$\frac{\partial u_2(r,t)}{\partial t} = D_2 \frac{\partial^2 u_2(r,t)}{\partial r^2}, \quad a < r \leq b, \; t > 0 \qquad (14)$$

with the boundary conditions,

$$u_1(a,t) = u_2(a,t) \text{ for } t > 0 \tag{15}$$

$$D_1\left(\frac{1}{r}\frac{\partial u_1}{\partial r} - \frac{u_1}{r^2}\right) = D_2\left(\frac{1}{r}\frac{\partial u_2}{\partial r} - \frac{u_2}{r^2}\right) \text{ at } r = a \tag{16}$$

$$u_2(b,t) = 0$$

$$u_1(r,0) = u_2(r,0) = rC$$

and $u_1(r,t)$ is finite at $r = 0$.

The solutions for the two regions are

$$C_1(r,t)=\frac{2bC}{r}\sum_{n=1}^{\infty}\frac{1}{\phi(\alpha_n)}\text{Sin } r\alpha_n \text{ Sin } a\alpha_n \text{ Sin}\left\{k(b-a)\alpha_n\right\}e^{-D_1\alpha_n^2 t} \tag{17}$$

and

$$C_2(r,t)= \frac{2bC}{r}\sum_{n=1}^{\infty}\frac{1}{\phi(\alpha_n)} \text{Sin}^2 a\alpha_n \text{ Sin}\left\{k(b-r)\alpha_n\right\}e^{-D_1\alpha_n^2 t} \tag{18}$$

where $k = \sqrt{\frac{D_1}{D_2}}$ and the α_n's are the roots of

$$D_2\left\{ka\alpha \text{ Cot } k(b-a)\alpha + 1\right\} + D_1\left\{a\alpha \text{ Cot } a\alpha - 1\right\} = 0 \tag{19}$$

along with the common roots of

$$\text{Sin } a\alpha = 0 \quad \text{and} \quad \text{Sin}\{k(b-a)\alpha\} = 0 \tag{20}$$

if $\frac{k(b-a)}{a}$ is rational.

Since $\frac{k(b-a)}{a}$ is a very small quantity in the case under consideration, the common roots of Equation 20 will be large. Since we are concerned with only the lowest value of α_n, we need to be concerned with only the roots of Equation 19.

$D_2 \gg D_1$ because the stress field of the grain boundary interacts with the point defects and they are attracted and bound to the grain boundary with a certain energy (33, p. 448). This force of attraction and its effects on diffusion of impurity atoms migrating to a single dislocation tilt boundary is known from the work of Webb (29). This theory can not be extended to large angle grain boundaries, because the dislocation model can not be applied to such boundaries. Furthermore, at the present time, no experimental data are available on the diffusion coefficient for defects moving toward the boundary due to the interaction with the stress field.

The lowest root of Equation 19 was evaluated for different grain sizes assuming typical values of $\frac{D_2}{D_1} = 10^2$ and the stressed region b-a = 10^{-2} cm. The annealing rate constant

$$K = \alpha_1^2 D_1 \tag{21}$$

Figure 2 shows a plot of the rate constant K against the number of grains/cm^2. The dependence is seen to be almost linear up to $b-a < \frac{a}{6}$. Beyond that, the curve deviates appreciably from linearity. In other words, the annealing rate will be directly proportional to the number of grain boundaries if and only if the stress field of the boundaries exert attractive forces which are only of a short range.

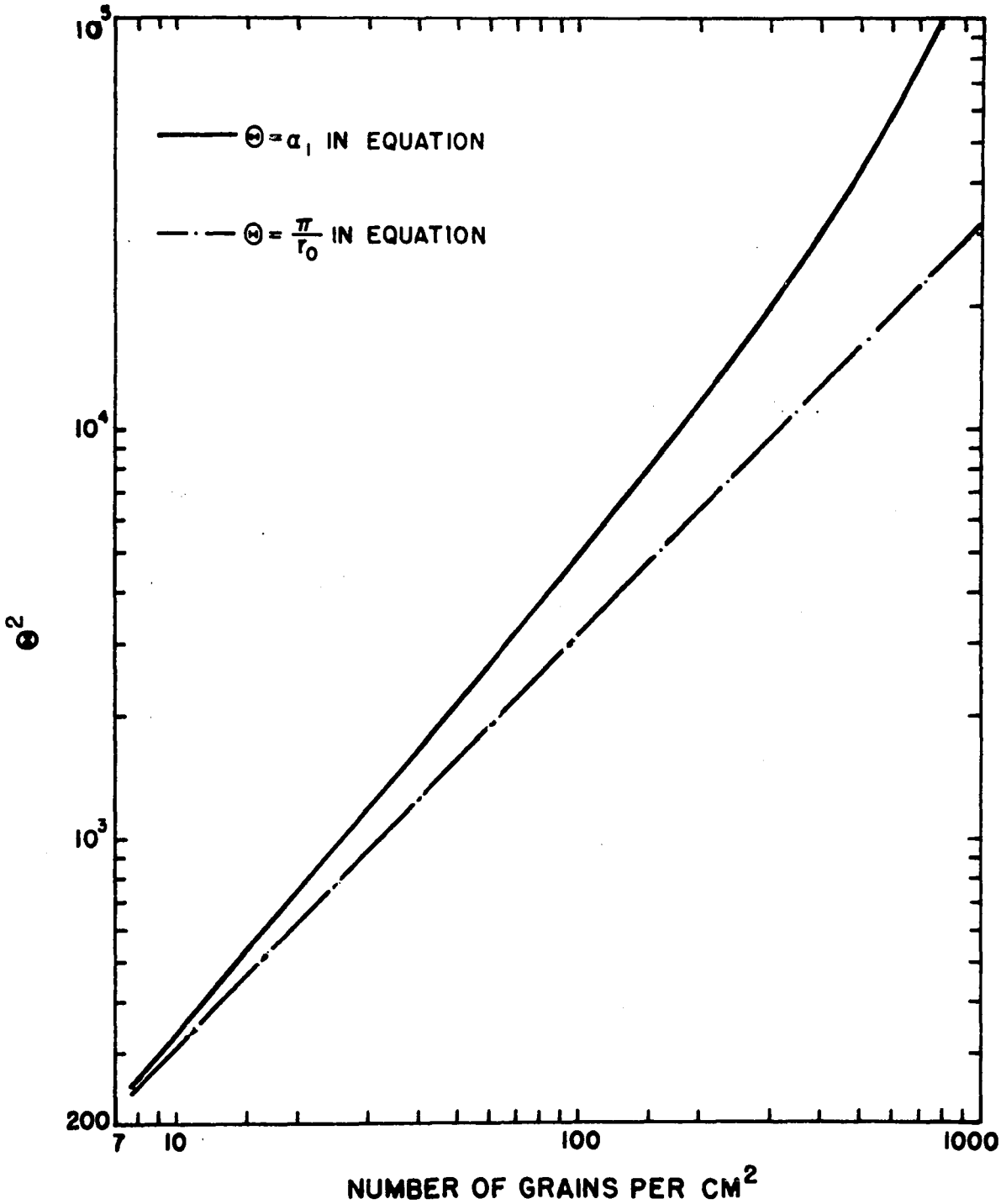

Figure 2. Theoretical curves showing the dependence of the annealing rate on the grain size

IV. EXPERIMENTAL INVESTIGATION

A. Specimens

Bismuth was chosen for this investigation for two reasons. Firstly, the rate of radiation damage is known to be highest in bismuth among metals (15, p. 115), which means that measurable changes in its electrical properties are possible even at relatively low radiation flux. Secondly, the electrical resistance of bismuth is comparatively large so that precise measurement of electrical resistivity is not difficult even on small samples.

Five polycrystalline rods, each 1.25 cm in diameter and 8.35 cm in length were bought from the Monocrystal Company, Cleveland, Ohio. They were grown from 99.999 per cent chemically pure bismuth with controlled grain sizes. Along with these five polycrystals, a single crystal also was used for this investigation, which was obtained from the Ames Laboratory. It was grown perpendicular to the C-axis and this fact was later confirmed by X-ray diffraction.

The polycrystals were carefully machined on a precision shaping machine and were cut with a jeweller's saw into rectangular specimens, approximately 0.5 cm x 0.25 cm x 8.35 cms, in size. They were then polished with sapphire and diamond paste and were etched with dilute Nitric acid.

The surface of the specimens were then observed under a microscope and the grain size for each specimen was determined by comparing the observed surface with the ASTM standards (34).

B. Electrical Circuit

The d.c circuit used for measurement of electrical resistivity is shown schematically in Figure 3. The six samples were connected in series and were supplied from a d.c. power unit. The probes for potential drop measurements in the specimens were spaced two inches apart. All the electrical contacts to the samples were made with lead-bismuth solder (39.9 per cent Pb, 60.1 per cent Bi) which has a very low resistivity. The potential drop in each specimen was recorded continuously on a Brown-Honeywell multipoint recorder. The current measurements were made by recording continuously the voltage across a known resistance on a Varian recorder. The direction of the flow of current could be changed at equal intervals using a two-way switching mechanism which simultaneously changed the polarity of the two recorders also. This change of current direction eliminated the formation of thermal gradients along the length of the specimens. By averaging the measurements for the two opposite directions of current flow, the effect due to the thermoelectric potential also was eliminated.

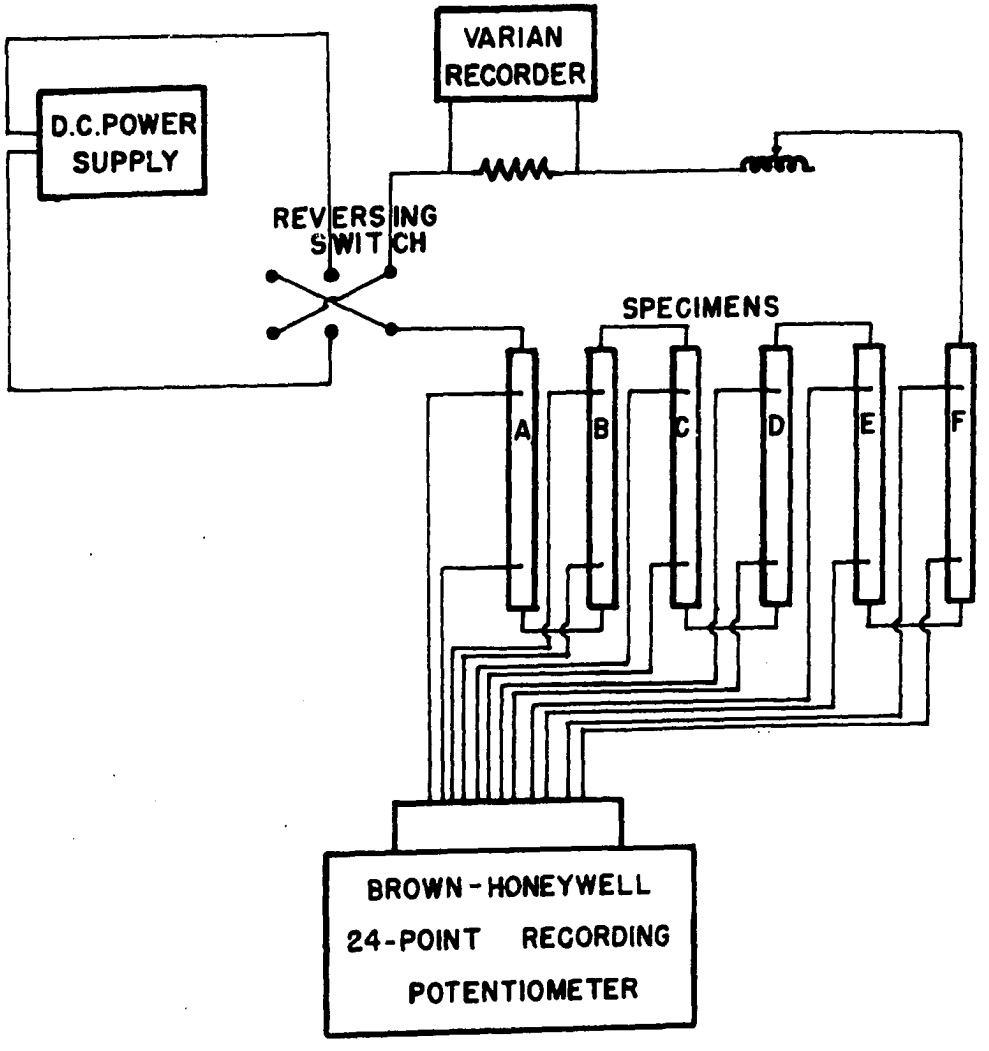

Figure 3. Schematic diagram of the electrical circuit

C. Cooling Circuit

Figure 4 shows a sketch of the circuit used for the irradiation of the specimens at a constant temperature of 12°C inside the central irradiation cavity of the UTR-10. Deionized water cooled in the storage tank was pumped through 1/4 inch diameter aluminum tubes wound in the shape of a square box. This box was thermally insulated from the graphite walls of the irradiation cavity using 3/32 inch thick plexiglass plates. All the six specimens were mounted around a plexiglass frame and placed inside the aluminum tubing box. This box was then sealed with another plexiglass sheet to avoid temperature changes due to air currents. The temperatures of the samples were measured continuously during the experiment using calibrated copper-constantan thermocouples connected to the samples.

D. Pre-irradiation Measurements

The electrical resistivities of the samples were measured at room temperature for a wide range of current passing through the specimens. The measurements were made for both the directions of current flow and the averaged results are shown in Figure 16 in the Appendix. The steep increase of the resistivity for currents lower than 60 milliamperes was

Figure 4. Schematic diagrams showing the cooling circuit for reactor irradiation

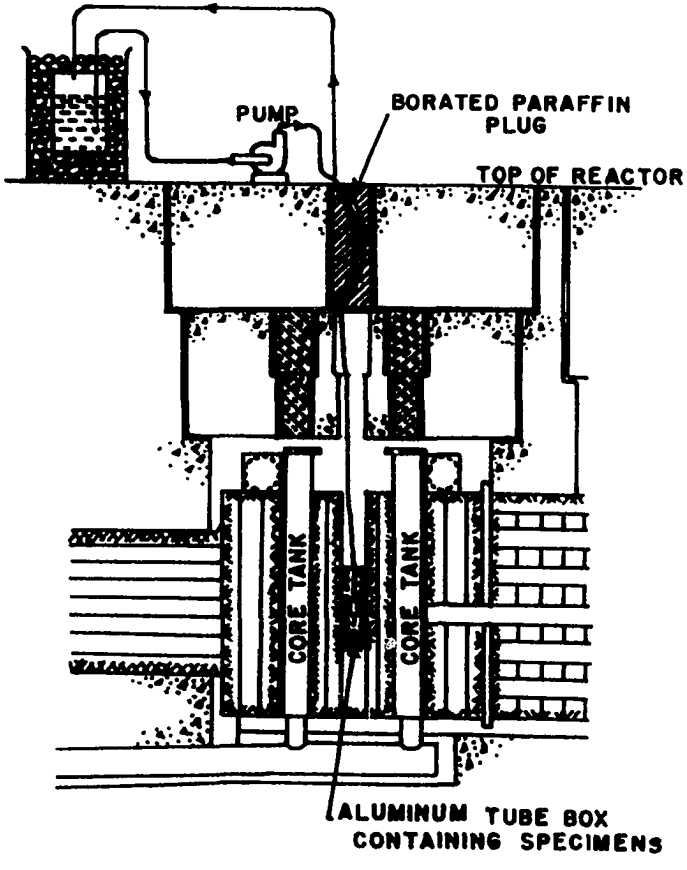
PUMP
BORATED PARAFFIN PLUG
TOP OF REACTOR
CORE TANK
CORE TANK
ALUMINUM TUBE BOX CONTAINING SPECIMENS

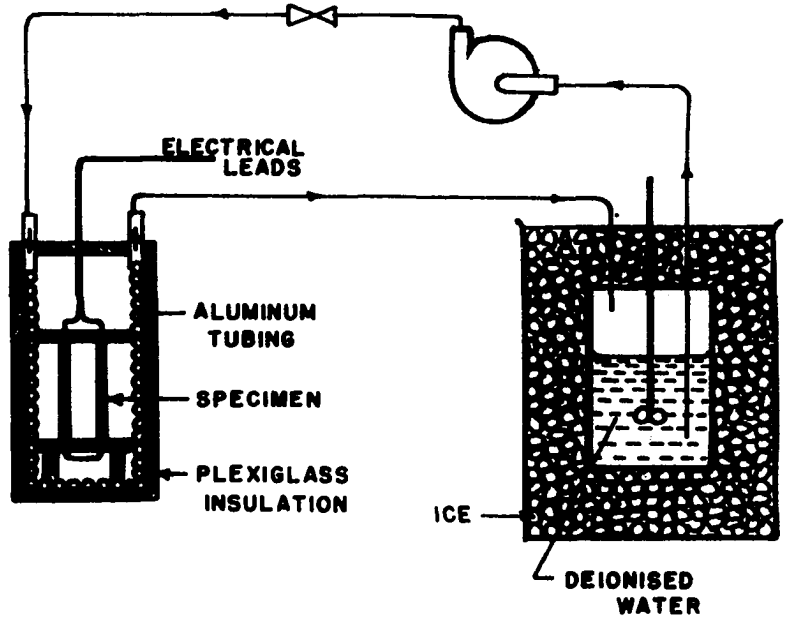
ELECTRICAL LEADS
ALUMINUM TUBING
SPECIMEN
PLEXIGLASS INSULATION
ICE
DEIONISED WATER

because of the effect of contact resistances. In order to minimize this effect the later experiments used a current of about 85 milliamperes.

Slight temperature changes could be anticipated during the irradiation experiments. In order to be able to correct for the effect of these temperature changes on the resistivity, the resistivity changes of the specimens were measured in the temperature range 0°C to 60°C, by external heating. The results are shown in Figure 17 in the Appendix.

E. Reactor Irradiation and Annealing

The specimens were kept inside the cooling coil box and the box then placed inside the irradiation hole in line with the center of the fuel region where the neutron flux peaks to a maximum. The top concrete plug of the reactor was replaced by a borated paraffin plug canned in aluminum. The coolant tubes and the electrical leads were lead out of the reactor through a curved hole inside the paraffin plug. Additional shielding was provided on top of the reactor with cadmium sheets and paraffin and lead bricks.

Ice-cold deionized water was circulated through the cooling coils and the steady state temperature obtained was 12°C. The reactor was then brought to the peak power level of 10 kW. The irradiation was continued for almost 10 hours

until the resistivity of all the specimens reached saturation which amounted to an integrated neutron flux of 1×10^{16} neutrons/cm^2. The temperature, the current and the potential drops across the specimens were recorded during the irradiation. The reactor was then shut down and the 12°C temperature was maintained in order to observe the annealing of the resistivity increase due to the irradiation. The resistivity and temperature data were again recorded for nearly 7 hours. The circulating water was then quickly heated to raise the temperature of the specimens to 40°C. The measurement of recovery of electrical conductivity was then repeated for this temperature for another 8 hours.

The temperature coefficient of resistivity was then measured for these partially annealed specimens and the temperature coefficient was found to be just the same as before irradiation. Therefore it was concluded that the temperature corrections to the irradiated specimens could be made using the temperature coefficients of the unirradiated specimens.

F. Gamma Irradiation

In order to see if the gamma flux in the reactor could have made any significant contribution to the electrical resistivity, a polycrystalline specimen of bismuth was placed

inside the radiation cavity of the 1.4 Curie, cobalt-60 irradiation facility at Iowa State University. The irradiation was carried on for almost six days at the room temperature and the resistivity and temperature measurements were made as before.

V. RESULTS

A. Reduction of Data

The data collected in the reactor irradiation and subsequent annealing and also during the gamma irradiation are given in Tables 2 through 8 of the Appendix.

The time of irradiation was assumed to have started at the instant at which the reactor reached the power level of 10 KW. The potential drop listed is the average for the two opposing directions of current flow. All the resistivity values were corrected for the effect of temperature changes, using the temperature coefficient of resistivity determined earlier for each specimen and the resistivity for all the measurements were brought to $12^{o}C$.

B. Reactor Irradiation and Annealing Data

Figures 5 through 7 give the resistivity curves of all the six specimens during the irradiation and annealing at the two temperatures $12^{o}C$ and $40^{o}C$. The general trend of the curves is clearly what can be expected. The increase in resistivity during the irradiation deviates from linearity due to the annealing of the damage taking place in conjunction with its production and soon reaches a steady saturation level

Figure 5. Change in electrical resistivity with time for specimens A and B

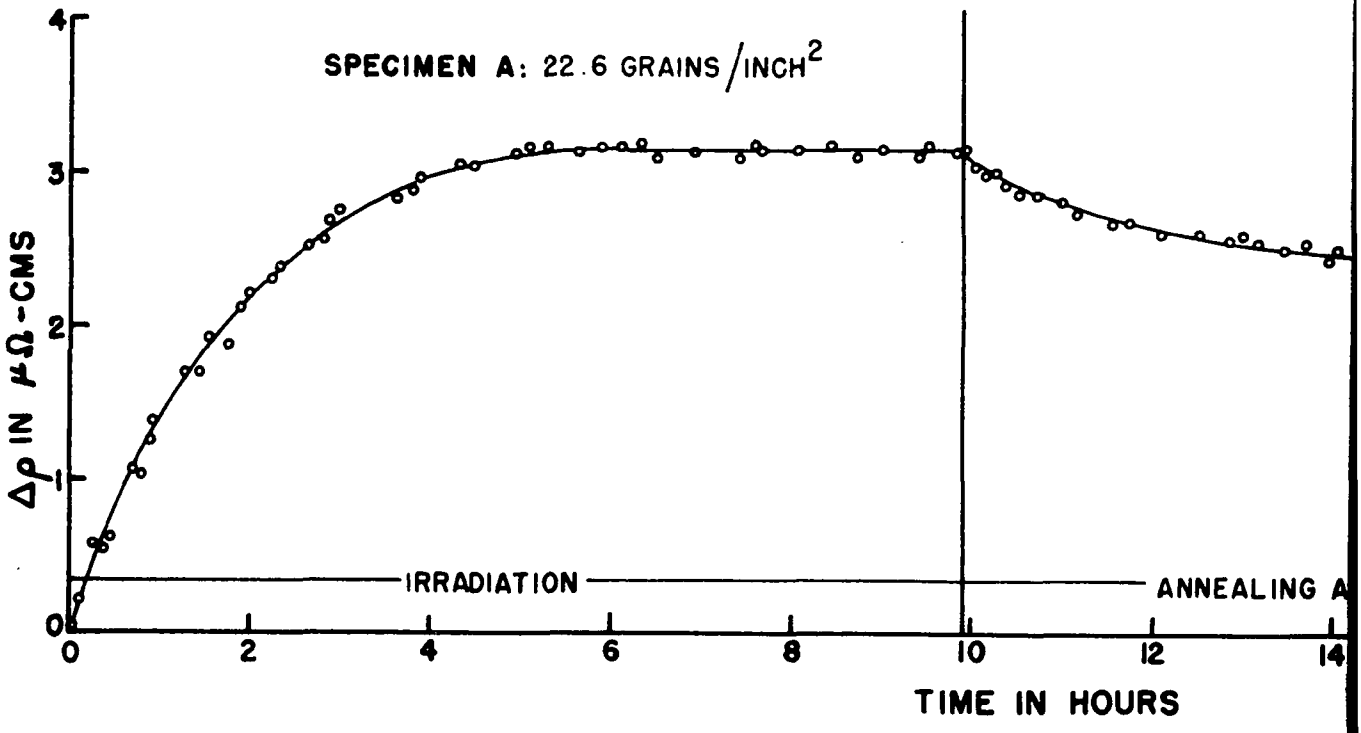
SPECIMEN A: 22.6 GRAINS/INCH²
Δρ IN μΩ-CMS
IRRADIATION
ANNEALING A
TIME IN HOURS

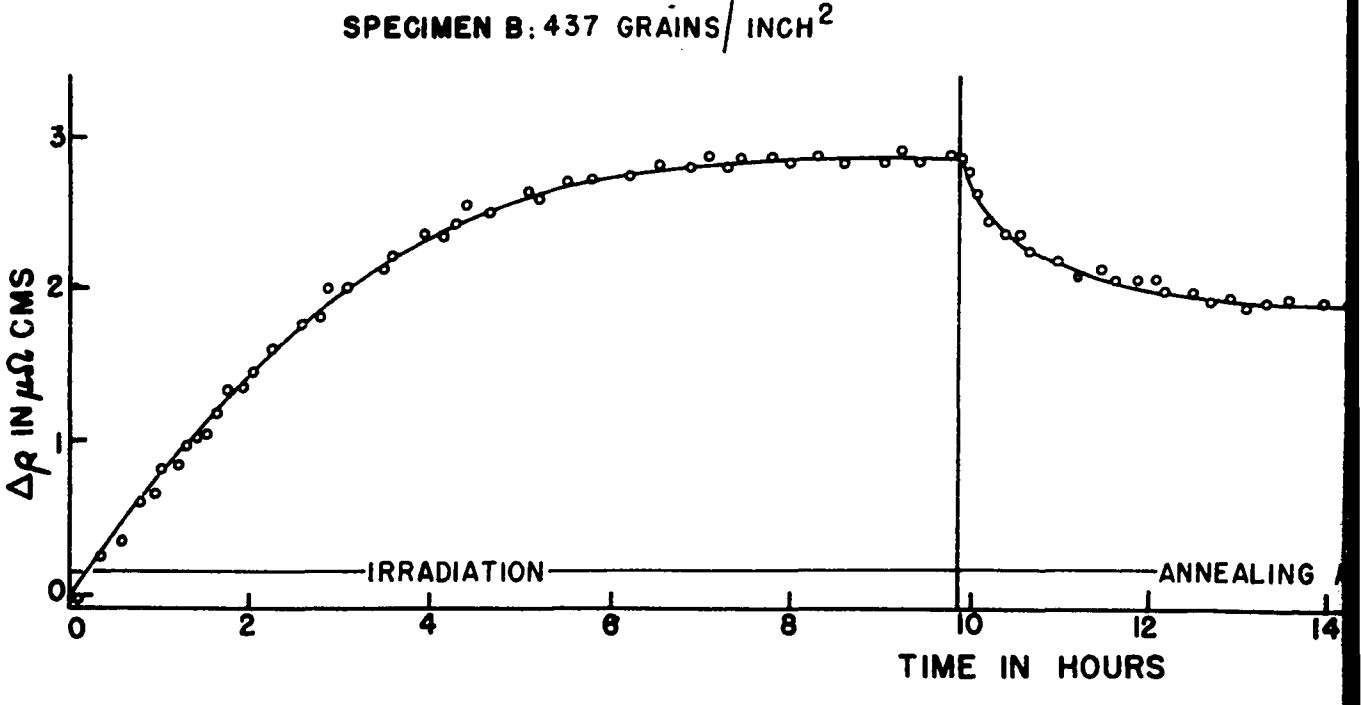
SPECIMEN B: 437 GRAINS/ INCH²
Δρ IN μΩ CMS
IRRADIATION
ANNEALING
TIME IN HOURS

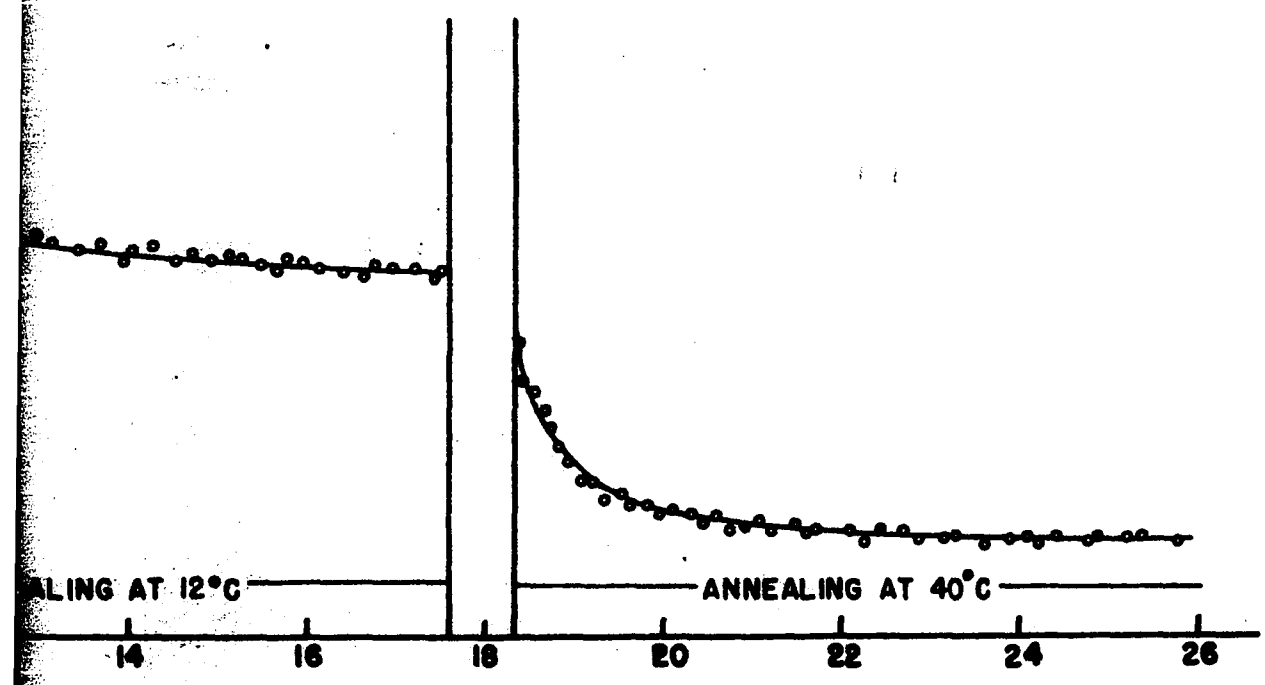
ALING AT 12°C
ANNEALING AT 40°C
14
16
18
20
22
24
26

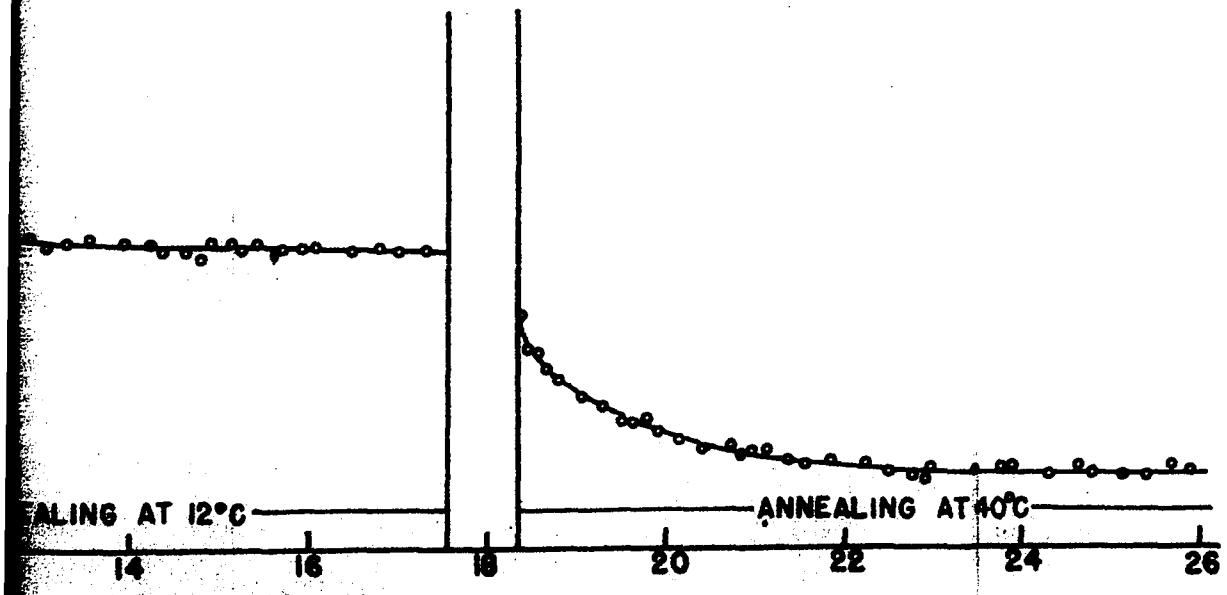
ALING AT 12°C
ANNEALING AT 40°C
14
16
18
20
22
24
26

Figure 6. Change in electrical resistivity with time for specimens C and D

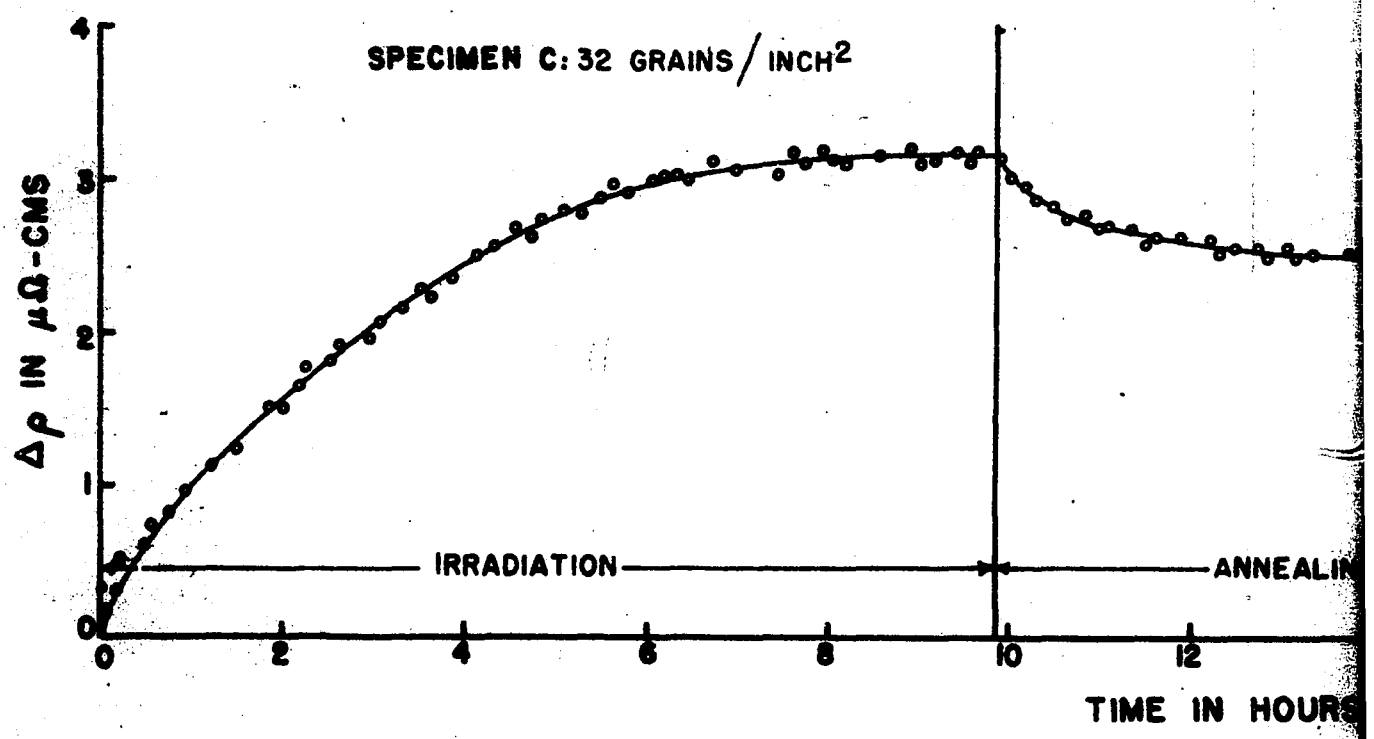
SPECIMEN C: 32 GRAINS / INCH²
Δρ IN μΩ-CMS
0
1
2
3
4
IRRADIATION
ANNEALIN
0
2
4
6
8
10
12
TIME IN HOURS

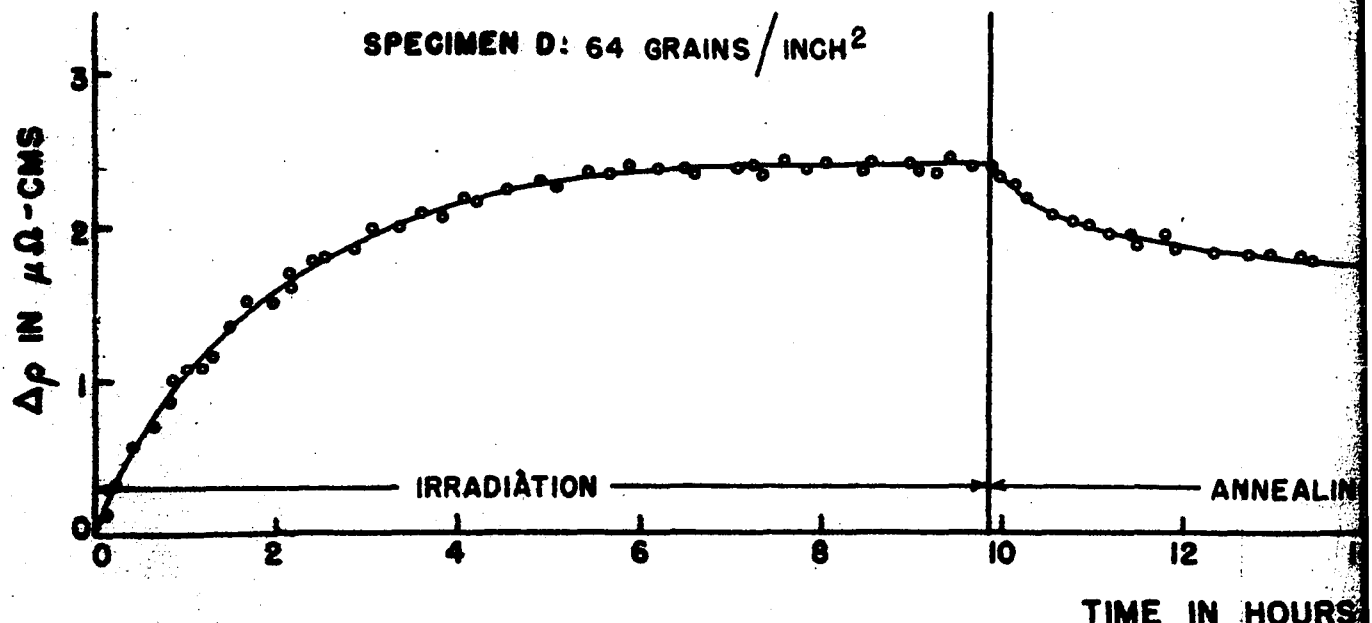
SPECIMEN D: 64 GRAINS / INCH²
Δρ IN μΩ-CMS
0
1
2
3
IRRADIATION
ANNEALIN
0
2
4
6
8
10
12
TIME IN HOURS

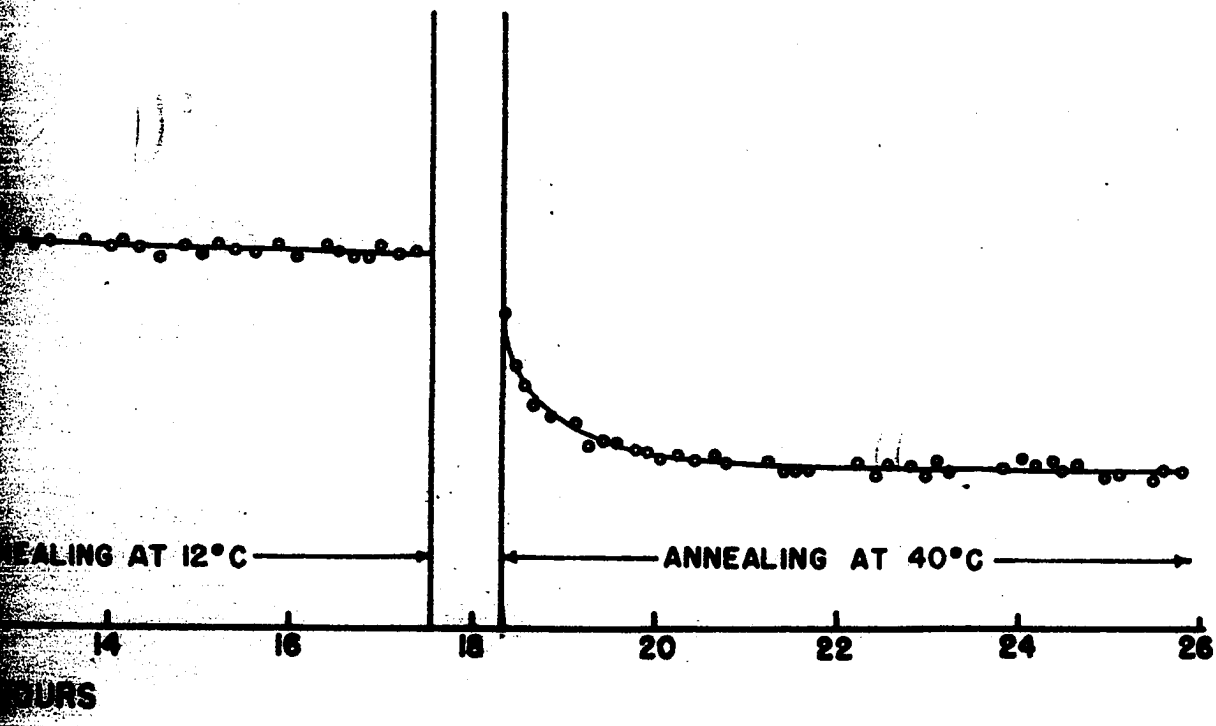
EALING AT 12°C
ANNEALING AT 40°C
14
16
18
20
22
24
26

OURS

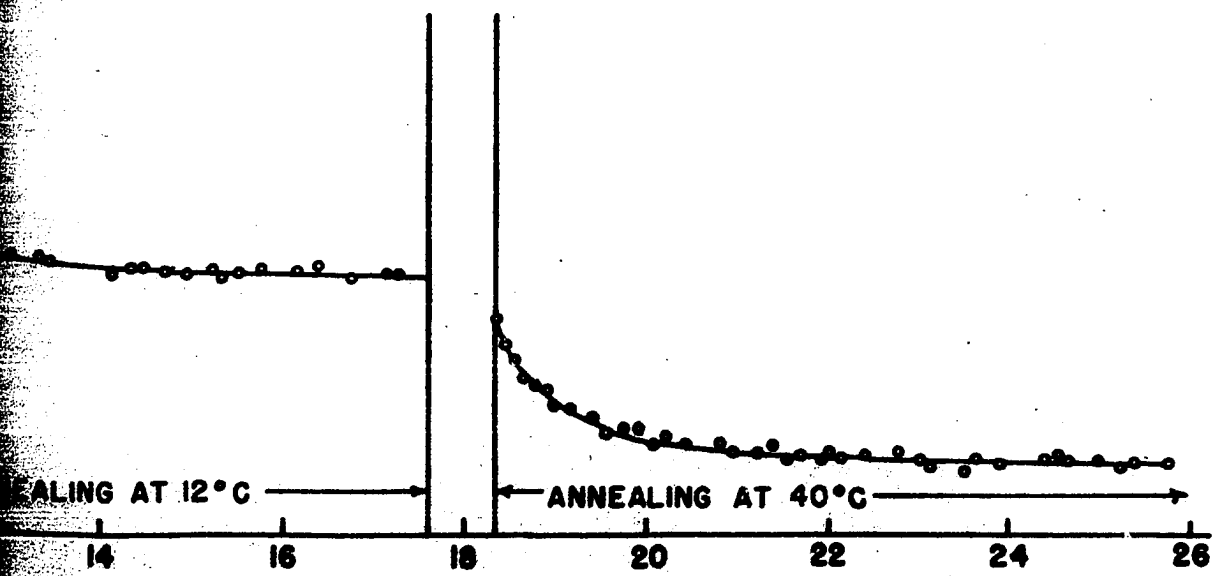
EALING AT 12°C
ANNEALING AT 40°C
14
16
18
20
22
24
26

OURS

Figure 7. Change in electrical resistivity with time for specimens E and F

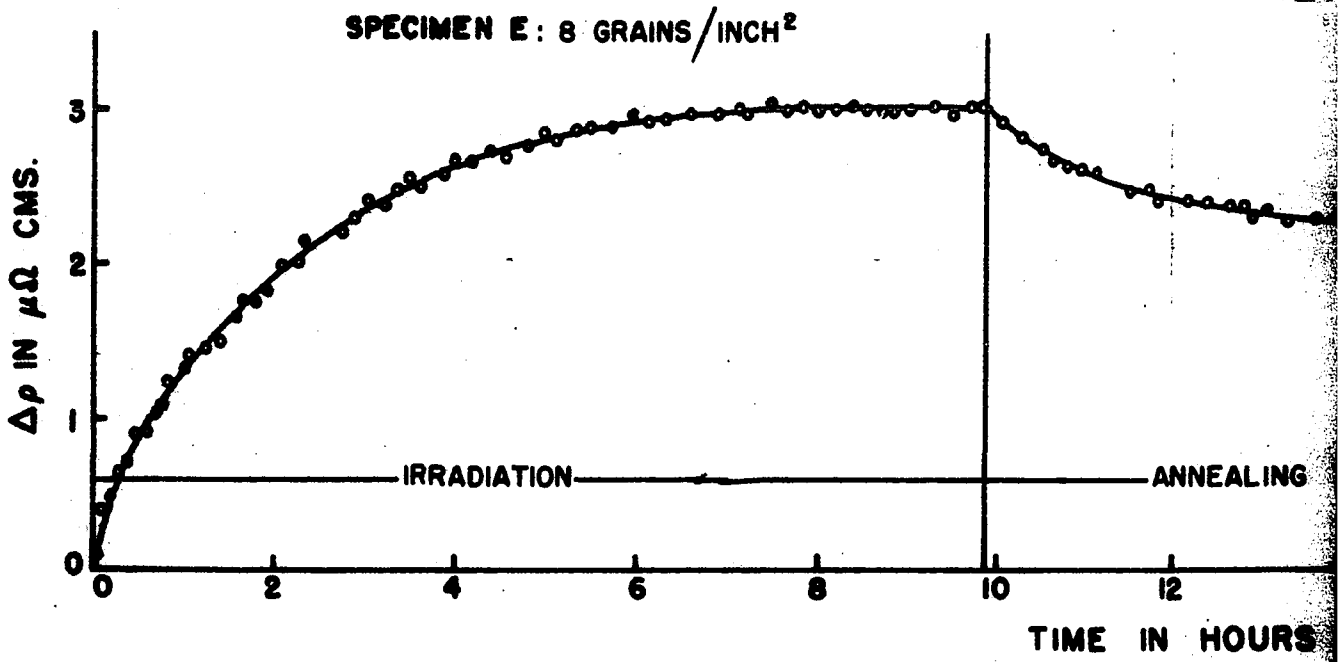
SPECIMEN E: 8 GRAINS/INCH²
Δρ IN μΩ CMS.
0
1
2
3
IRRADIATION
ANNEALING
0
2
4
6
8
10
12
TIME IN HOURS

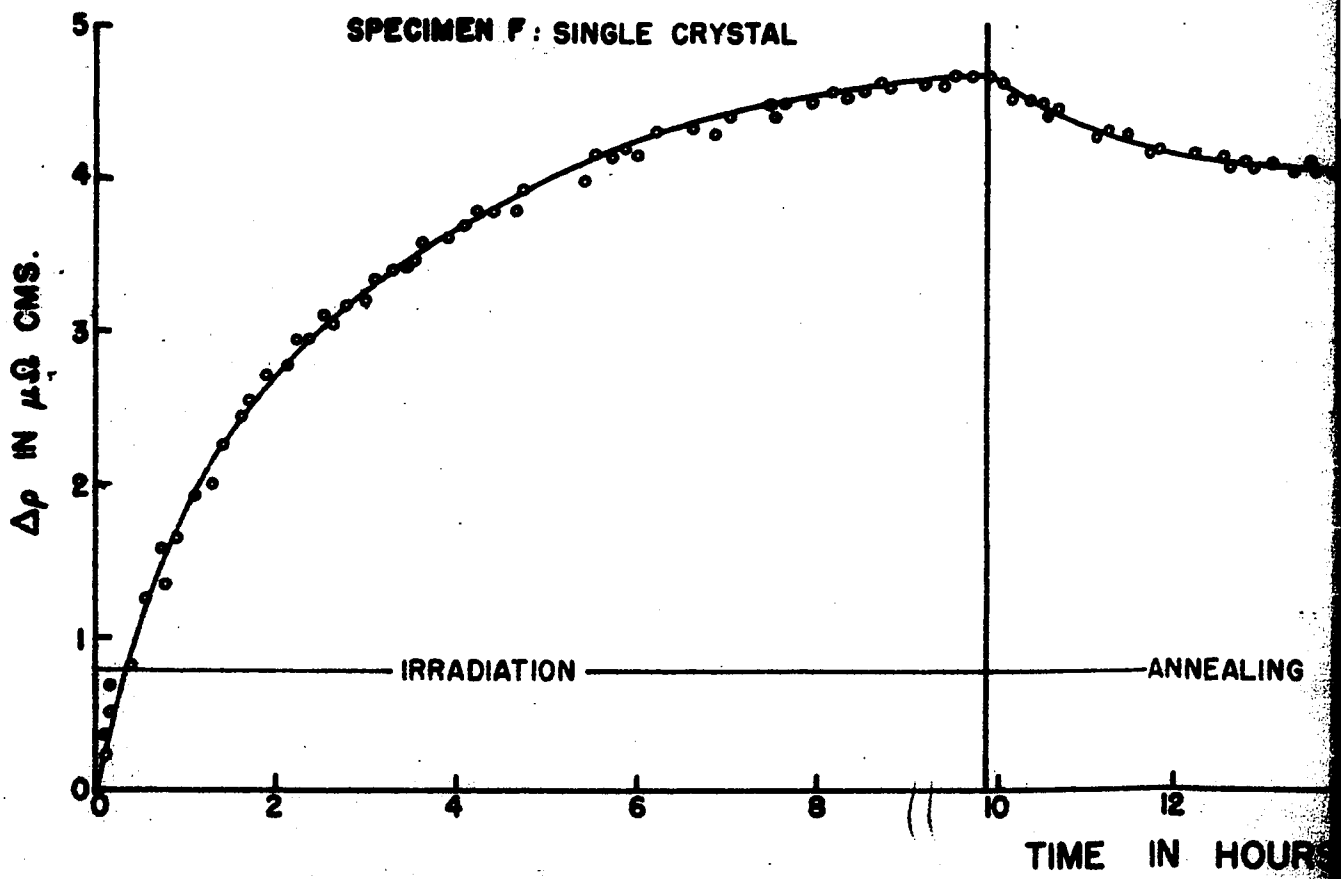
SPECIMEN F: SINGLE CRYSTAL
Δρ IN μΩ CMS.
0
1
2
3
4
5
IRRADIATION
ANNEALING
0
2
4
6
8
10
12
TIME IN HOURS

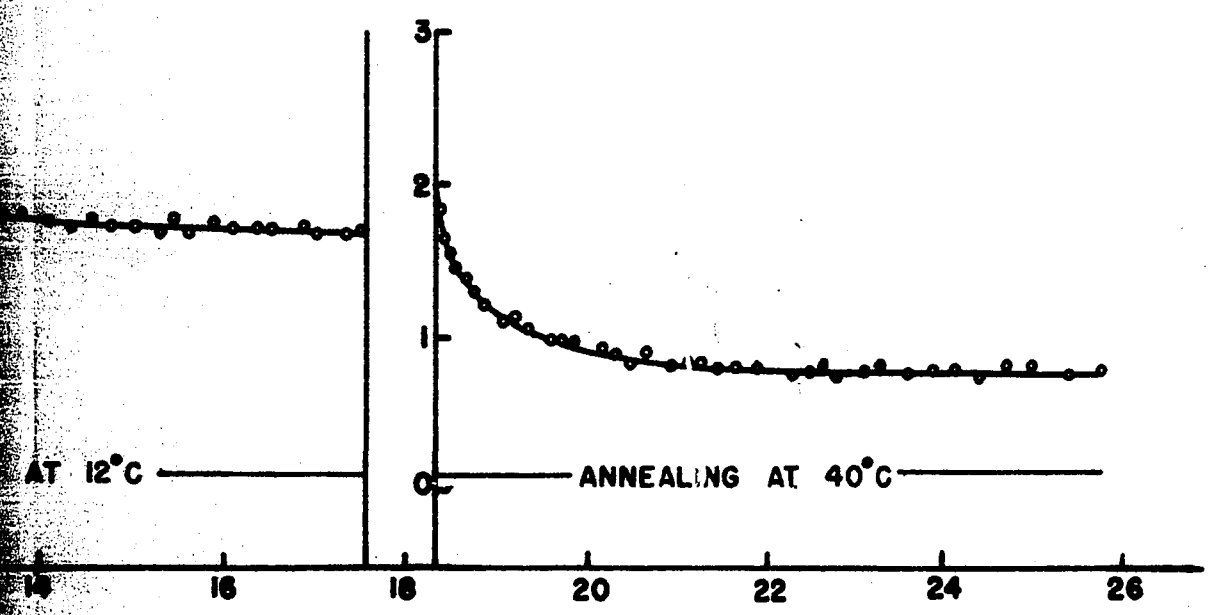
3
2
1
0
AT 12°C
ANNEALING AT 40°C
14
16
18
20
22
24
26

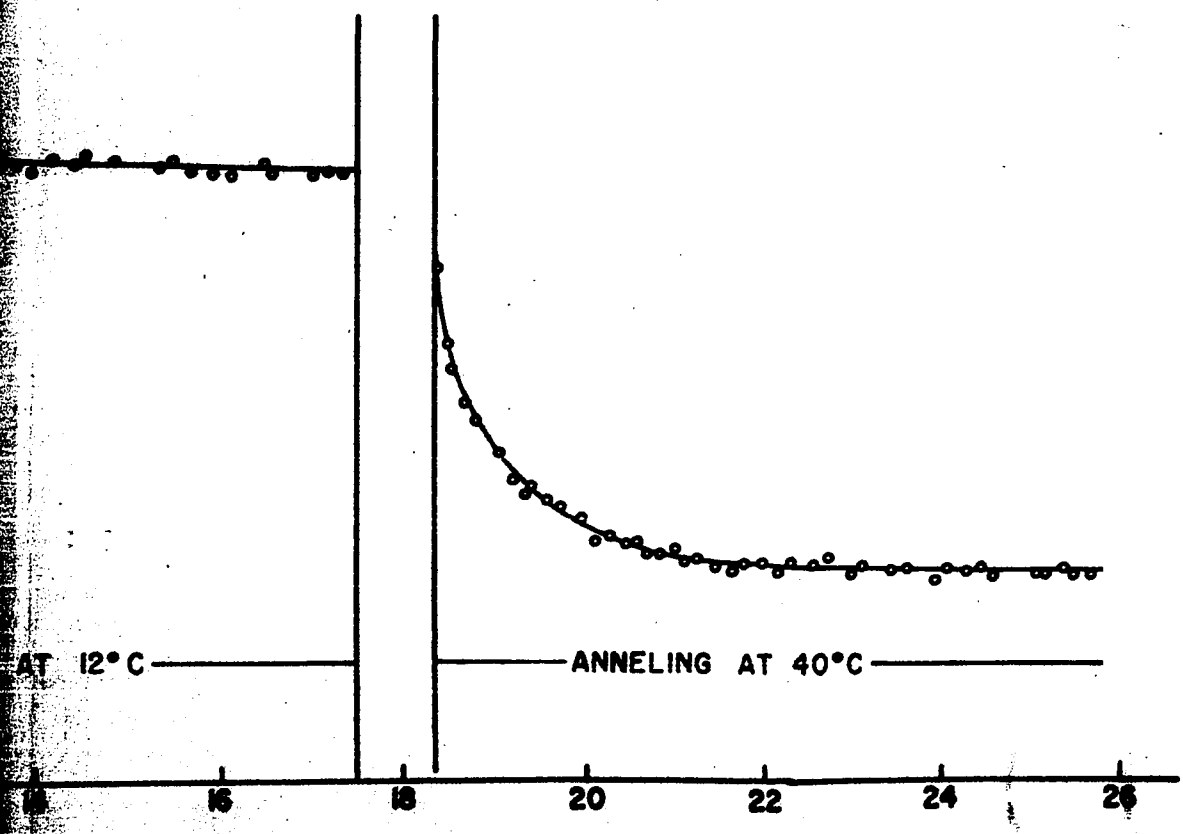
AT 12° C
ANNELING AT 40°C
16
18
20
22
24
26

because of the equilibrium between the production rate and the annealing rate. The total increase in the resistivity is more in the case of the single crystal than in the polycrystal which indicates that annealing is less in the former. The annealing curves show an exponential decrease and then level off to an equilibrium at each of the temperatures. Almost 75 per cent of the total resistivity increase annealed out during the annealing at 12°C and at 40°C.

C. Analysis of the Recovery Data

Literature shows that many different methods are available for analyzing the annealing data (16). Because of the reasons stated in Section II, the method of analysis used in this investigation is the same as the method used by Glower (27).

It is known from Matthiessen's rule that the total electrical resistivity is the sum of the resistivities due to each of the different ways of electron scattering. This applies clearly to the change in resistivity due to the introduction of defect structure in the material. The annealing of any particular kind of defect is a rate process given by

$$\frac{dN}{dt} = - \lambda N \qquad (22)$$

where N is the number of defects of a certain kind at any time t. The change in electrical resistivity $\Delta\rho$ due to this type of defect is proportional to N and so Equation 22 can be rewritten as

$$\frac{d(\Delta\rho)}{dt} = -\lambda(\Delta\rho) \tag{23}$$

On integration between proper limits, it is found that for a typical recovery curve as shown in Figure 8,

$$\ln \frac{\Delta\rho(t) - \Delta\rho_o}{\Delta\rho_{sat}} = -\lambda t \tag{24}$$

$\Delta\rho(t)$, $\Delta\rho_o$, and $\Delta\rho_{sat}$ are as shown in Figure 8.

The decay constant λ is also given by Equation 1. Therefore, if λ is known for a particular annealing process at two different temperatures, the activation energy and the rate constant K for this process can be determined.

The annealing curves for the six samples at 12°C and 40°C were replotted with $\ln \frac{\Delta\rho(t) - \Delta\rho_o}{\Delta\rho_{sat}}$ against time. These curves are shown in Figures 9 through 14.

These curves show two definite components with different half lives. These components were "stripped" from the total curve and their decay constants λ were determined.

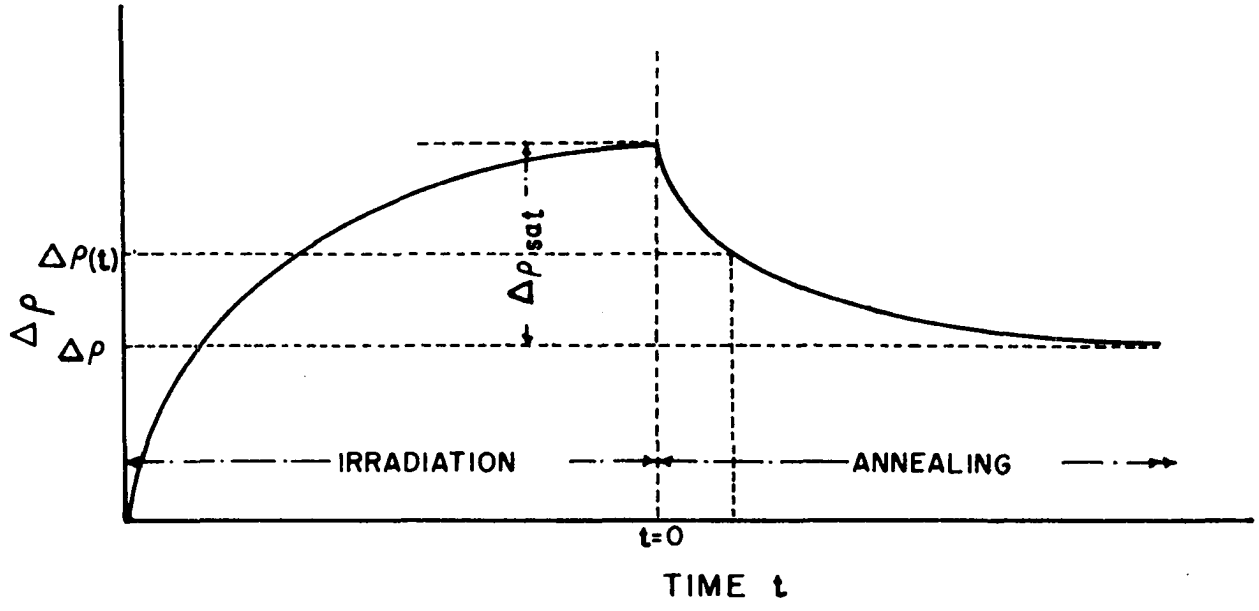

Figure 8. A typical irradiation and recovery curve showing the quantities used in Equation 24

Figure 9. Analysis of the annealing curves at 12°C and at 40°C for specimen A

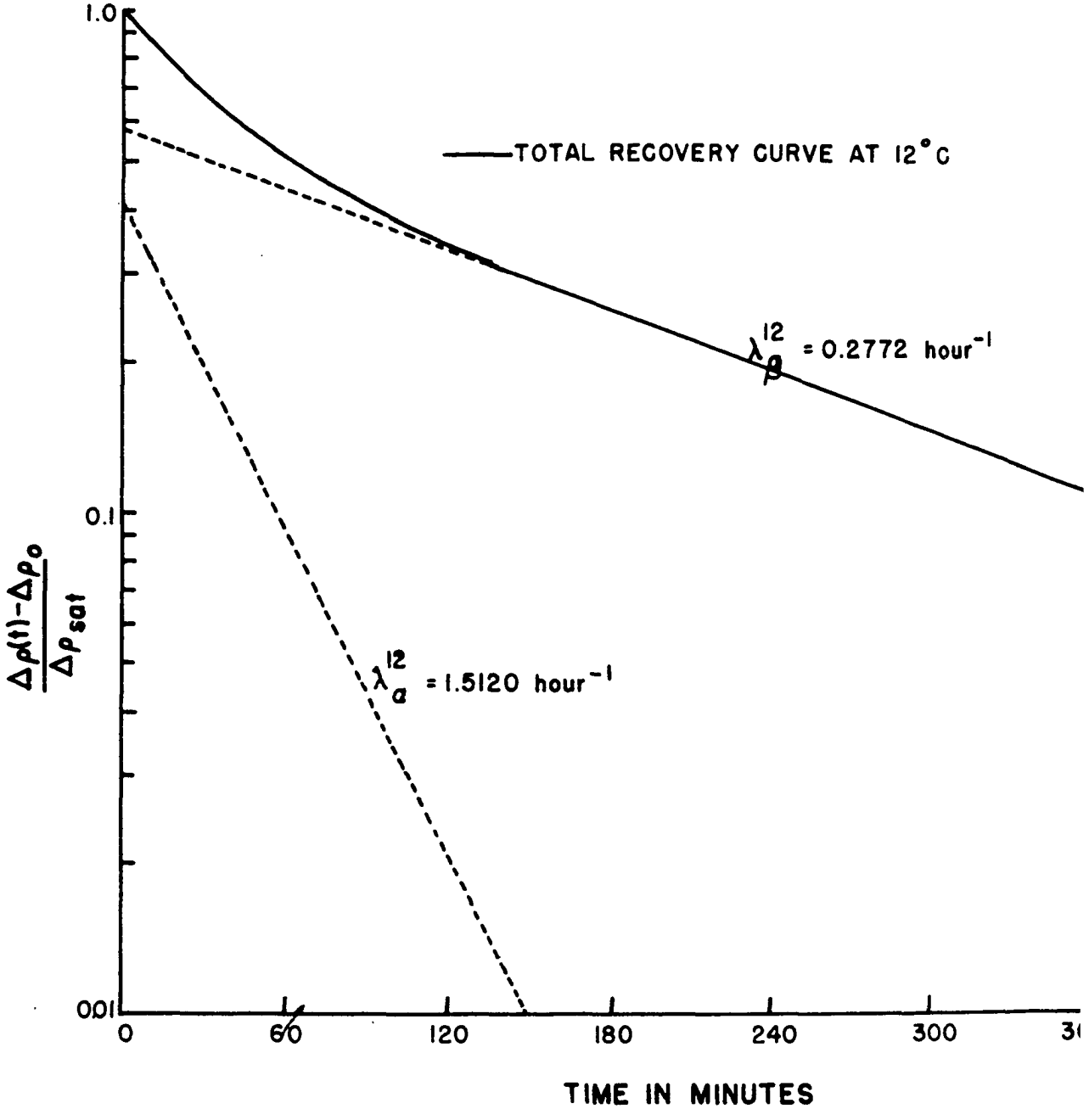
1.0
0.1
0.01
TOTAL RECOVERY CURVE AT 12°C
λ_β^{12} = 0.2772 hour^{-1}
λ_a^{12} = 1.5120 hour^{-1}
$\frac{\Delta\rho(t)-\Delta\rho_0}{\Delta\rho_{sat}}$
0
60
120
180
240
300
TIME IN MINUTES

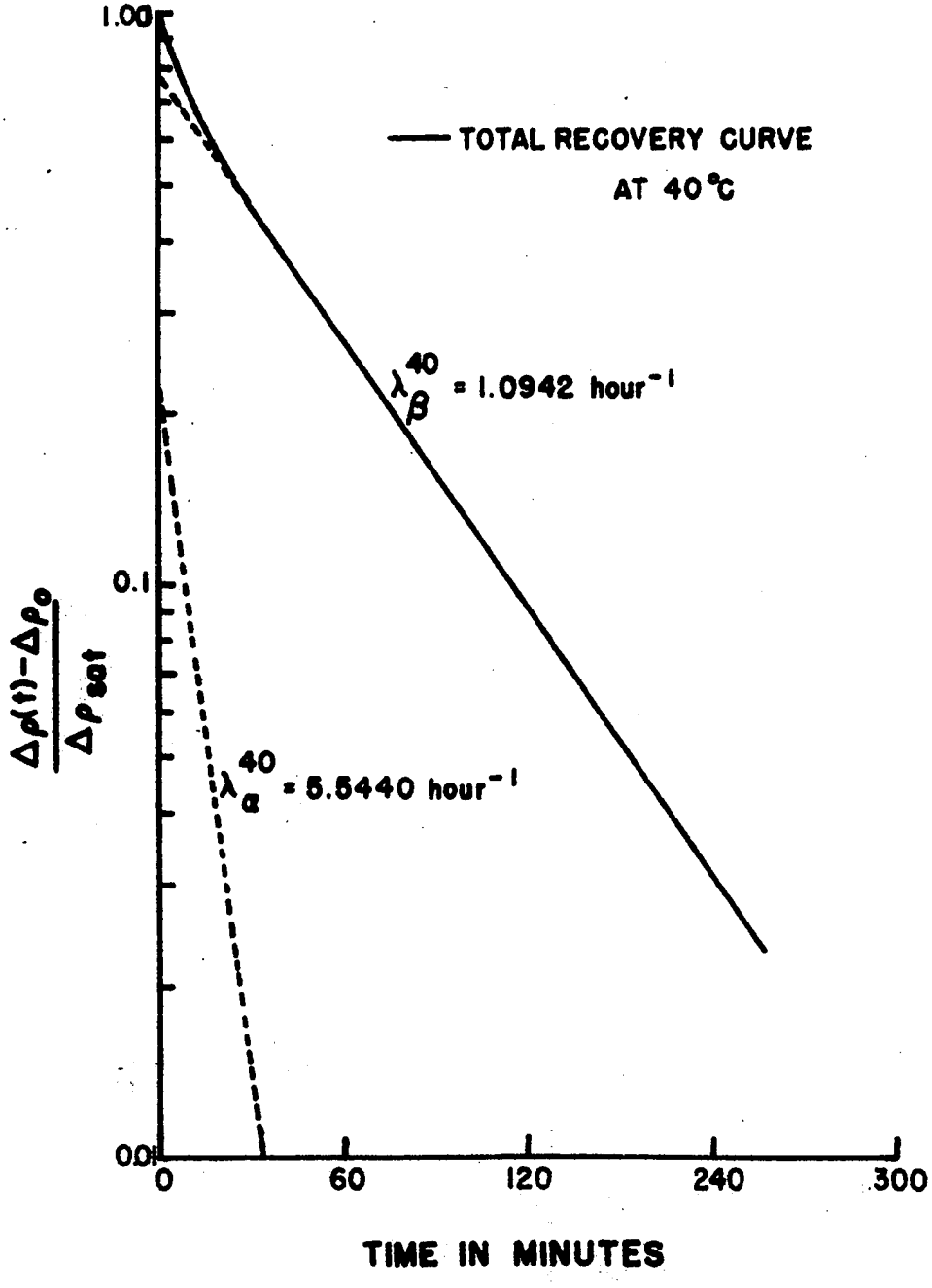
1.00
0.1
0.01
0
60
120
240
300
TOTAL RECOVERY CURVE
AT 40°C
λ_β^{40} = 1.0942 hour^{-1}
λ_α^{40} = 5.5440 hour^{-1}
$\frac{\Delta\rho(t)-\Delta\rho_0}{\Delta\rho_{sat}}$
TIME IN MINUTES

Figure 10. Analysis of the annealing curves at 12°C and at 40°C for specimen B

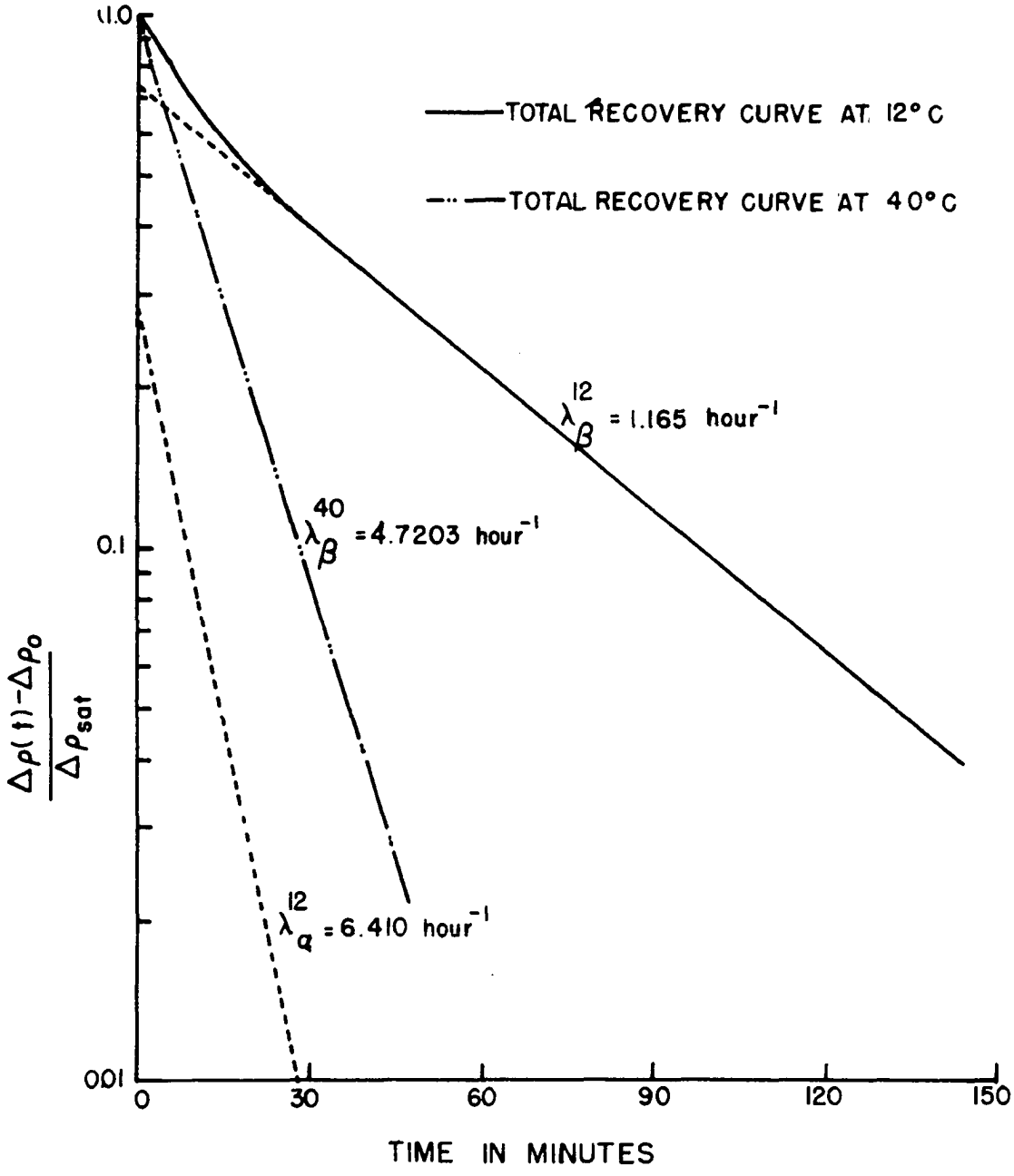
1.0
0.1
0.01
0
30
60
90
120
150
TIME IN MINUTES
$\frac{\Delta\rho(t)-\Delta\rho_0}{\Delta\rho_{sat}}$
TOTAL RECOVERY CURVE AT 12° C
TOTAL RECOVERY CURVE AT 40° C
λ_β^{12} = 1.165 hour^{-1}
λ_β^{40} = 4.7203 hour^{-1}
λ_α^{12} = 6.410 hour^{-1}

Figure 11. Analysis of the annealing curves at 12°C and at 40°C for specimen C

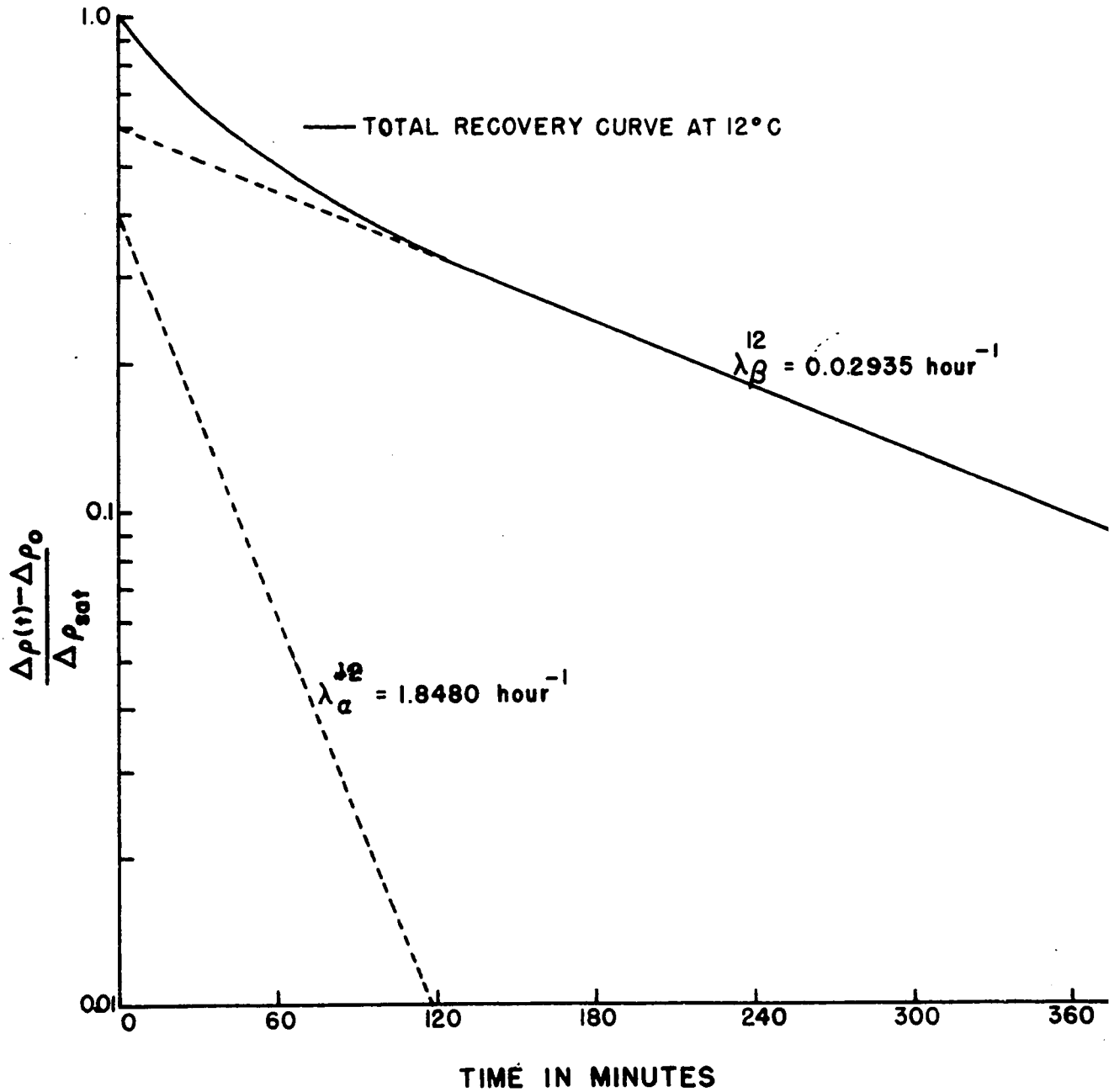
1.0
0.1
0.01
0
60
120
180
240
300
360
TOTAL RECOVERY CURVE AT 12°C
λ_{β}^{12} = 0.0.2935 hour^{-1}
λ_{α}^{12} = 1.8480 hour^{-1}
$\frac{\Delta\rho(t)-\Delta\rho_0}{\Delta\rho_{sat}}$
TIME IN MINUTES

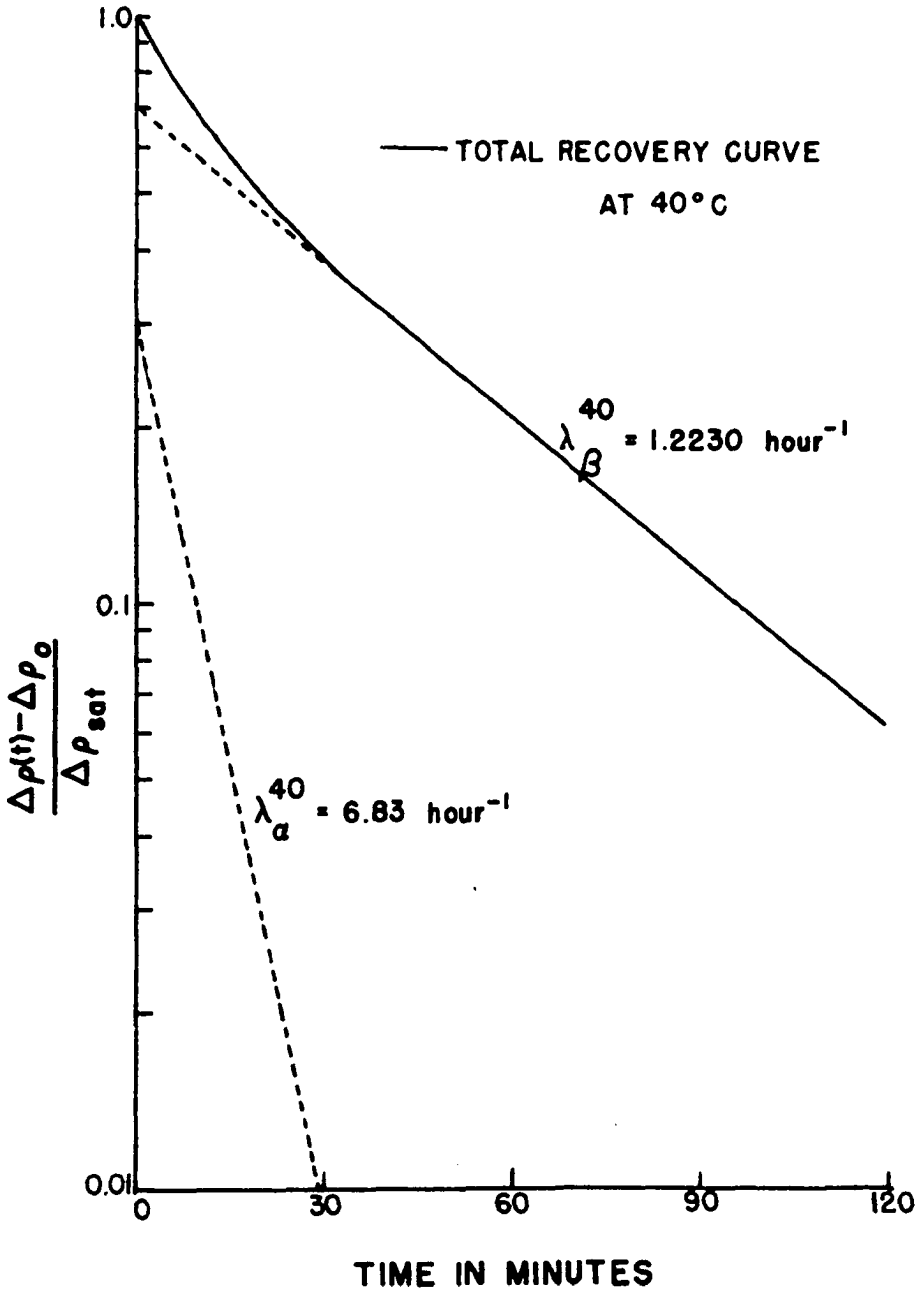
1.0
0.1
0.01
0
30
60
90
120
TOTAL RECOVERY CURVE
AT 40°C
λ_β^{40} = 1.2230 hour^{-1}
λ_α^{40} = 6.83 hour^{-1}
$\frac{\Delta\rho(t)-\Delta\rho_0}{\Delta\rho_{sat}}$
TIME IN MINUTES

Figure 12. Analysis of the annealing curves at 12°C and at 40°C for specimen D

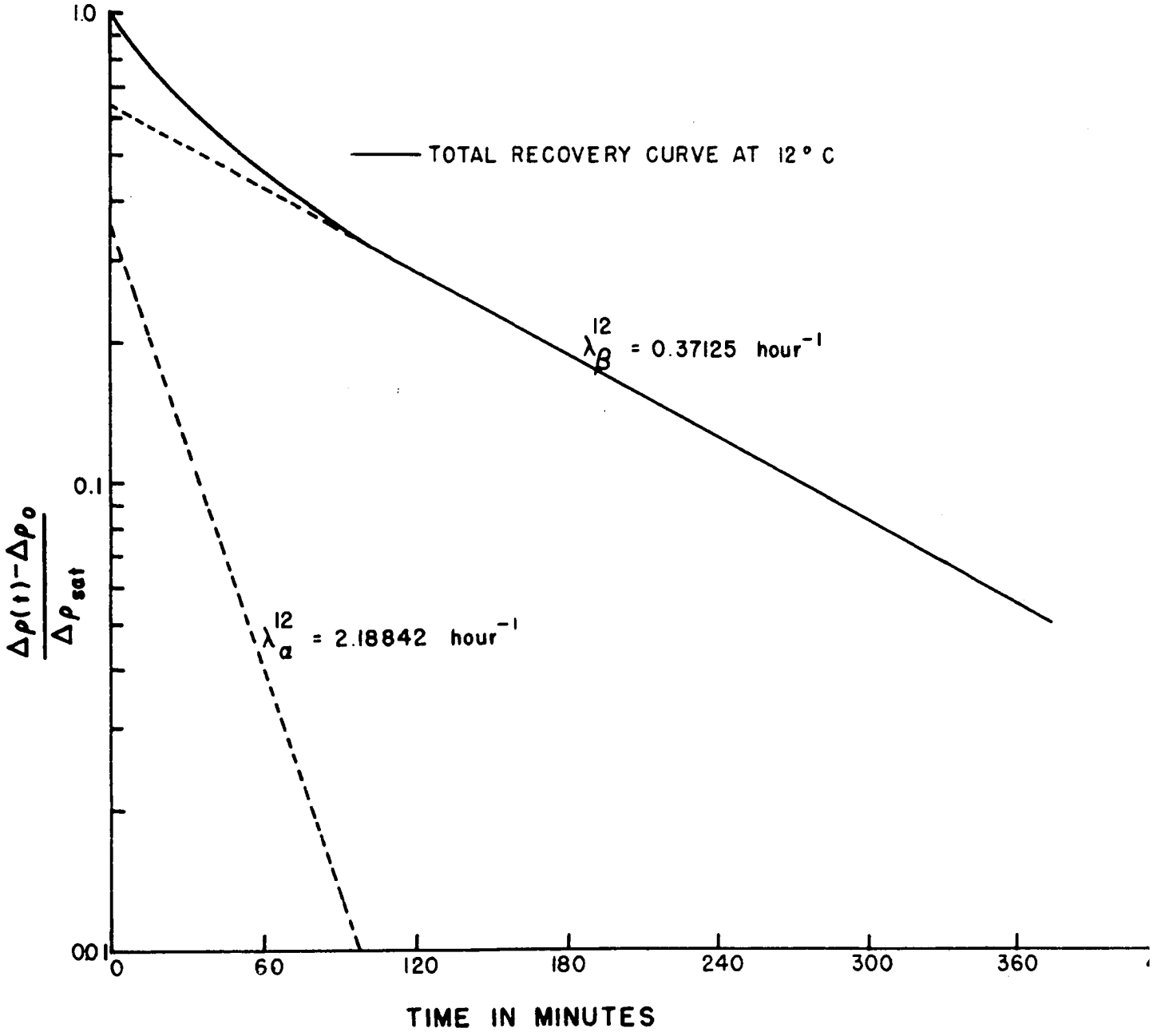
1.0
0.1
0.01
TOTAL RECOVERY CURVE AT 12° C
λ_β^{12} = 0.37125 hour^{-1}
λ_α^{12} = 2.18842 hour^{-1}
$\frac{\Delta\rho(t)-\Delta\rho_0}{\Delta\rho_{sat}}$
0
60
120
180
240
300
360
TIME IN MINUTES

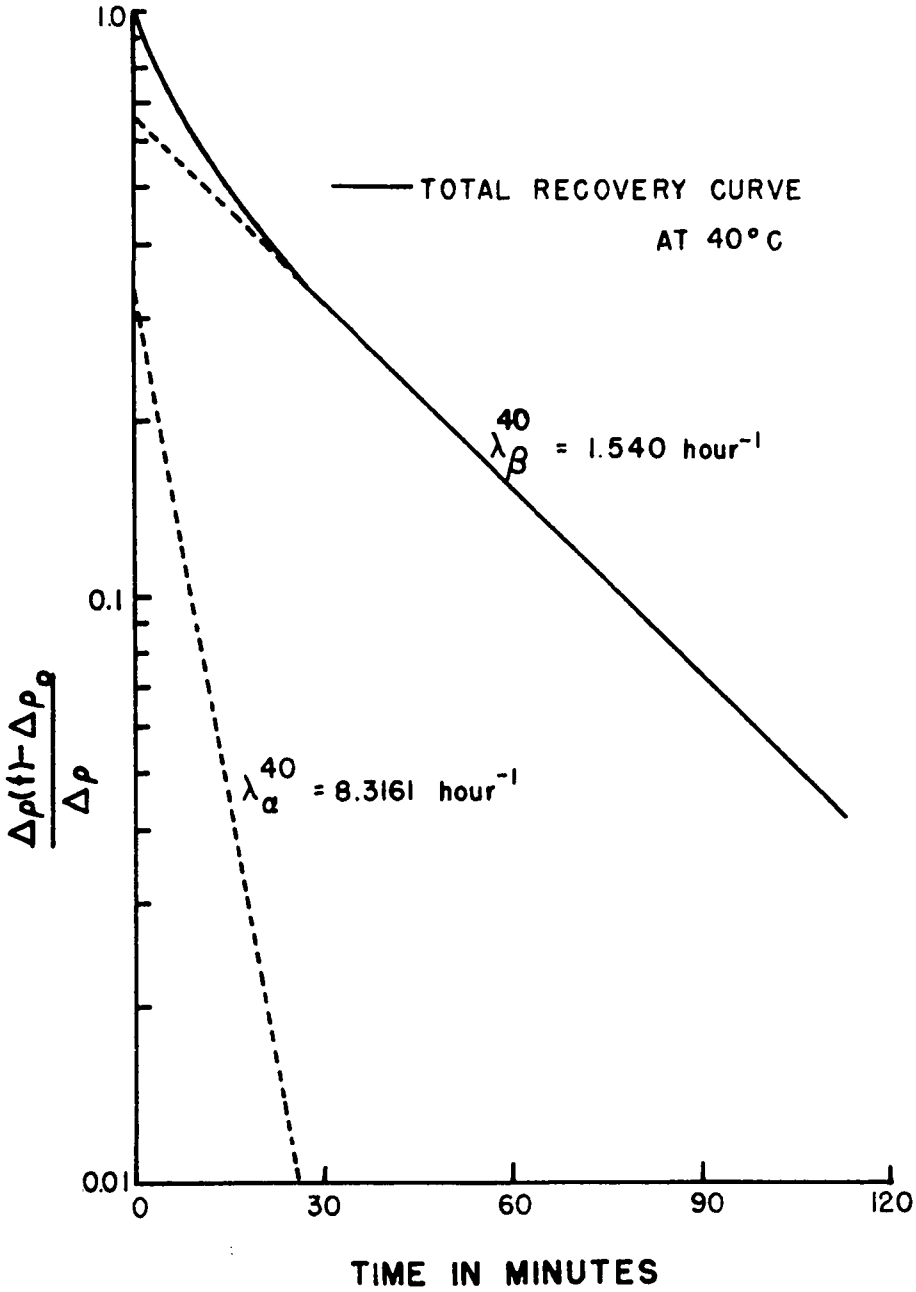
1.0
0.1
0.01
0
30
60
90
120
TOTAL RECOVERY CURVE
AT 40° C
λ_β^{40} = 1.540 hour^{-1}
λ_α^{40} = 8.3161 hour^{-1}
$\frac{\Delta\rho(t)-\Delta\rho_0}{\Delta\rho}$
TIME IN MINUTES

Figure 13. Analysis of the annealing curves at 12°C and at 40°C for specimen E

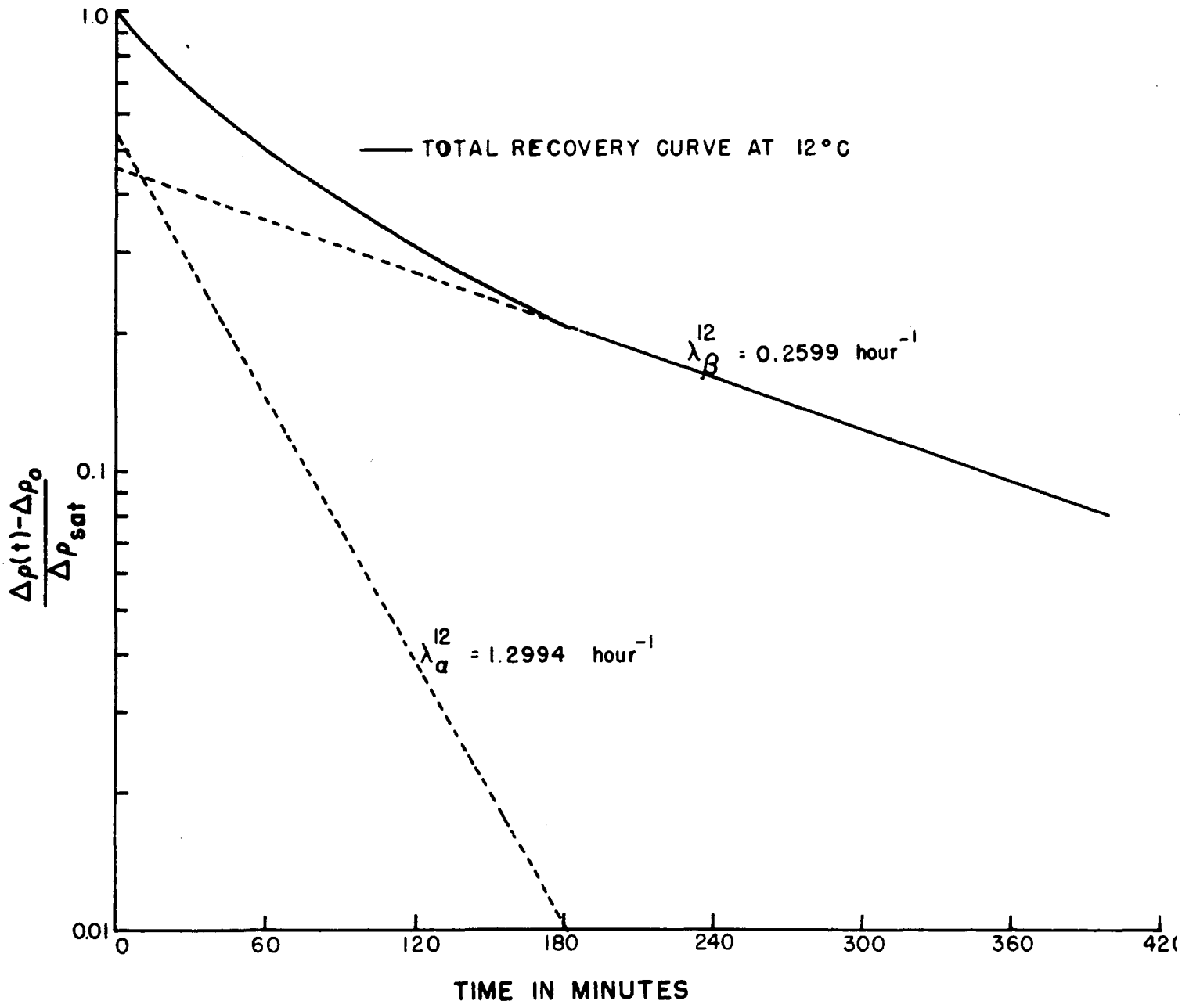
1.0
0.1
0.01
TOTAL RECOVERY CURVE AT 12°C
λ_{β}^{12} = 0.2599 hour^{-1}
λ_{α}^{12} = 1.2994 hour^{-1}
$\frac{\Delta\rho(t)-\Delta\rho_0}{\Delta\rho_{sat}}$
0
60
120
180
240
300
360
420
TIME IN MINUTES

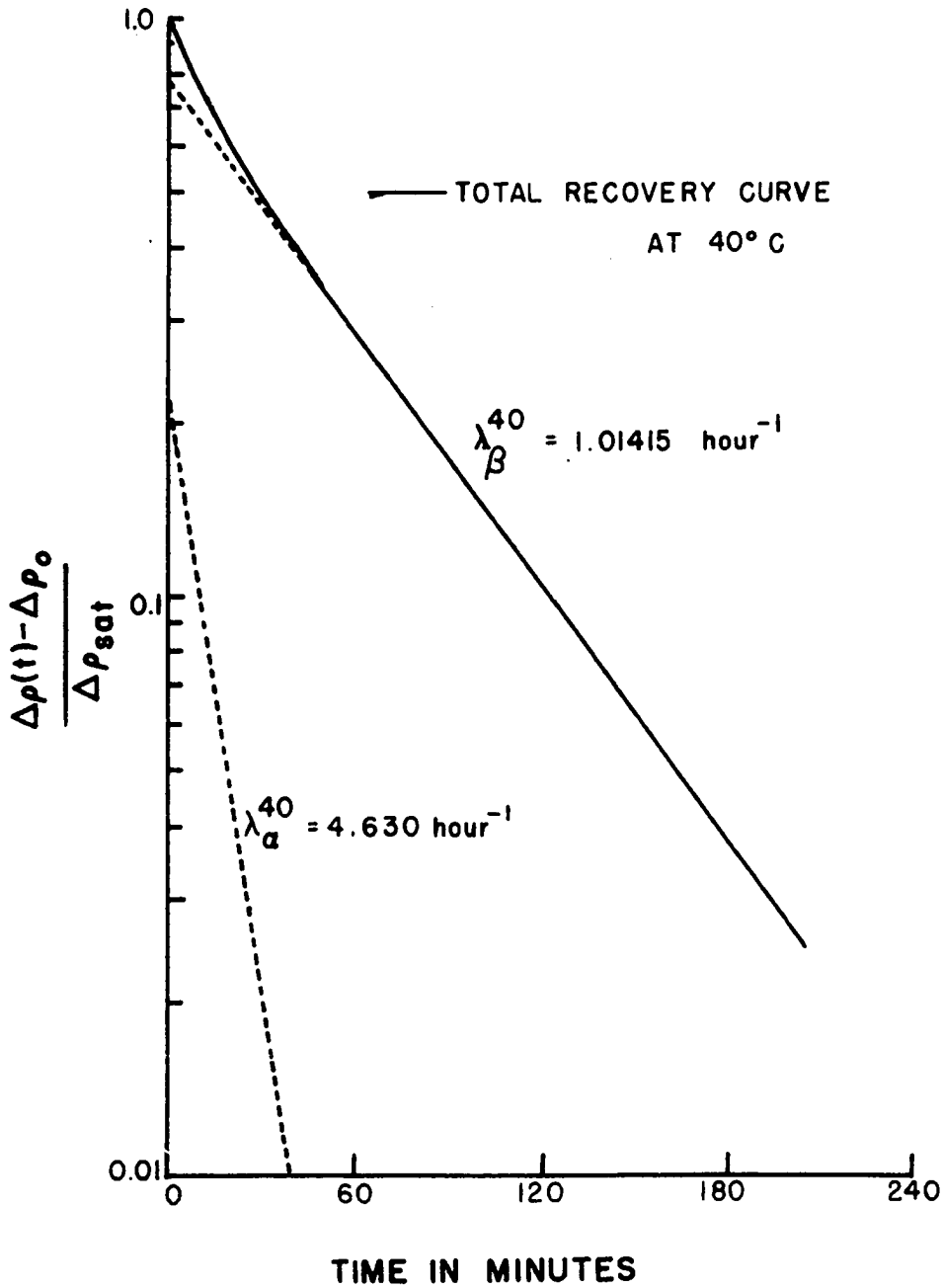
1.0
0.1
0.01
0
60
120
180
240
TOTAL RECOVERY CURVE
AT 40° C
λ_β^{40} = 1.01415 hour^{-1}
λ_α^{40} = 4.630 hour^{-1}
$\frac{\Delta\rho(t)-\Delta\rho_o}{\Delta\rho_{sat}}$
TIME IN MINUTES

Figure 14. Analysis of the annealing curves at 12°C and at 40°C for specimen F

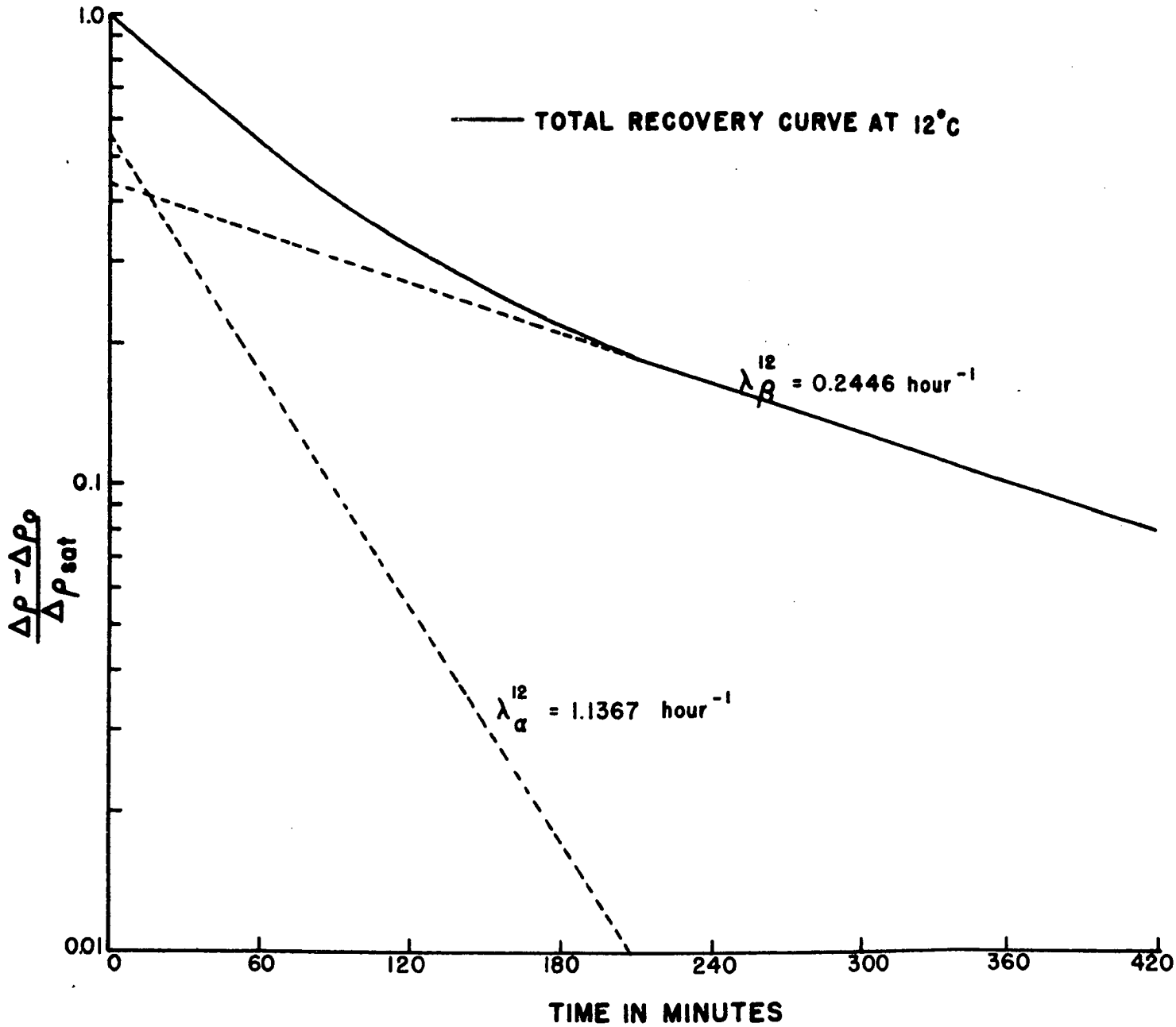
1.0
0.1
0.01
$\frac{\Delta\rho - \Delta\rho_0}{\Delta\rho_{sat}}$
TOTAL RECOVERY CURVE AT 12°C
λ_β^{12} = 0.2446 hour^{-1}
λ_α^{12} = 1.1367 hour^{-1}
0
60
120
180
240
300
360
420
TIME IN MINUTES

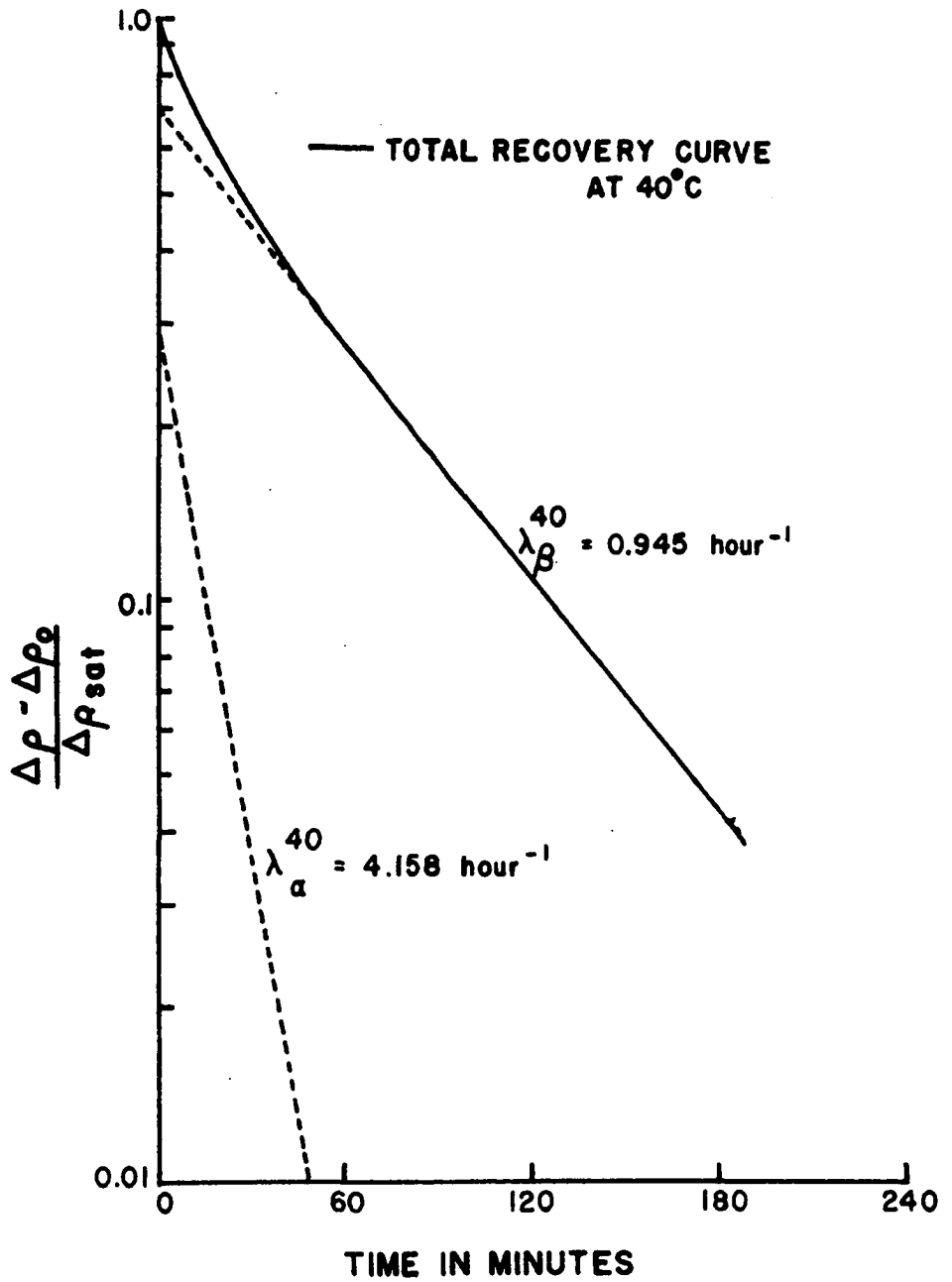
1.0
0.1
0.01
0
60
120
180
240
TOTAL RECOVERY CURVE AT 40°C
λ_β^{40} = 0.945 hour^{-1}
λ_α^{40} = 4.158 hour^{-1}
$\frac{\Delta\rho - \Delta\rho_0}{\Delta\rho_{sat}}$
TIME IN MINUTES

By assuming that each of these two components at the two temperatures represents the same process, and by labelling the shorter lived process α and the long-lived process β, the following equations may be written.

$$\lambda_{\alpha}^{12} = K_{\alpha}\, e^{-\frac{E_{\alpha}}{285\ k}} \qquad \lambda_{\beta}^{12} = K_{\beta}\, e^{-\frac{E_{\beta}}{285\ k}}$$

$$\lambda_{\alpha}^{40} = K_{\alpha}\, e^{-\frac{E_{\alpha}}{313\ k}} \qquad \lambda_{\beta}^{40} = K_{\beta}\, e^{-\frac{E_{\beta}}{313\ k}} \qquad (25)$$

$$\text{i.e.,} \frac{\lambda_{\alpha}^{40}}{\lambda_{\alpha}^{12}} = e^{3.643\ E_{\alpha}} \qquad \frac{\lambda_{\beta}^{40}}{\lambda_{\beta}^{12}} = e^{3.643\ E_{\beta}}$$

Here, λ_x^T = the decay constant of annealing process x at temperature $T^{\circ}C$

K_x = the rate constant of the annealing process x

E_x = the activation energy for annealing process x

From Equation 25, E_{α}, E_{β}, K_{α} and K_{β} for all the six specimens were determined and these values are tabulated in Table 1 along with the number of grains per $inch^2$ for each specimen.

Table 1. Annealing rate constants and activation energies

Specimen	No. of grains/inch^2	Annealing rates		Activation energies eV	
		$K_\alpha \times 10^{-6}$	$K_\beta \times 10^{-6}$	E_α	E_β
F	0[a]	1.8825	0.405	0.352	0.371
E	8	2.65	0.939	0.356	0.371
A	22.6	3.013	1.051	0.357	0.377
C	32.0	4.722	1.869	0.363	0.385
D	64.0	7.876	2.985	0.371	0.391
B	437	-	10.364	-	0.393

[a]The data from the single crystal was plotted at zero grains per square inch. This is not strictly valid because the crystal had finite dimensions.

D. Gamma Irradiation

The results of the gamma irradiation for six days on a polycrystalline specimen with 8 grains/inch^2 are tabulated in Table 8 of the Appendix. No change in the electrical resistivity was observed during the irradiation.

VI. DISCUSSION

The annealing rate constant for the α and β-components were plotted against the number of grain boundaries/inch^2 of the specimens. These plots are shown in Figure 15.

The dependence is undoubtedly linear as predicted by the theory. The dip that occurs at 22.5 grains/inch^2 must be because of some error in the determination of the number of grains in that specimen, especially since that dip occurs identically for both the α and the β-components.

The rate of increase of the annealing rate constants with the number of grains is estimated from Figure 15 to be 10^5/grain/inch^2 for the α-component and 3.6×10^4/grain/inch^2 for the β-component. This means that the α-component is more strongly dependent on the grain boundary sinks than in the case of the β-component. The activation energies for the two components are nevertheless, not much different from each other. Therefore, the number of defects of the kind taking part in the α-component of annealing must be larger than the number of defects of the kind involved in the β-component.

The activation energy for both the annealing components show a slight and gradual increase as the grain size becomes smaller (Table 1). This could be due to the increase in the

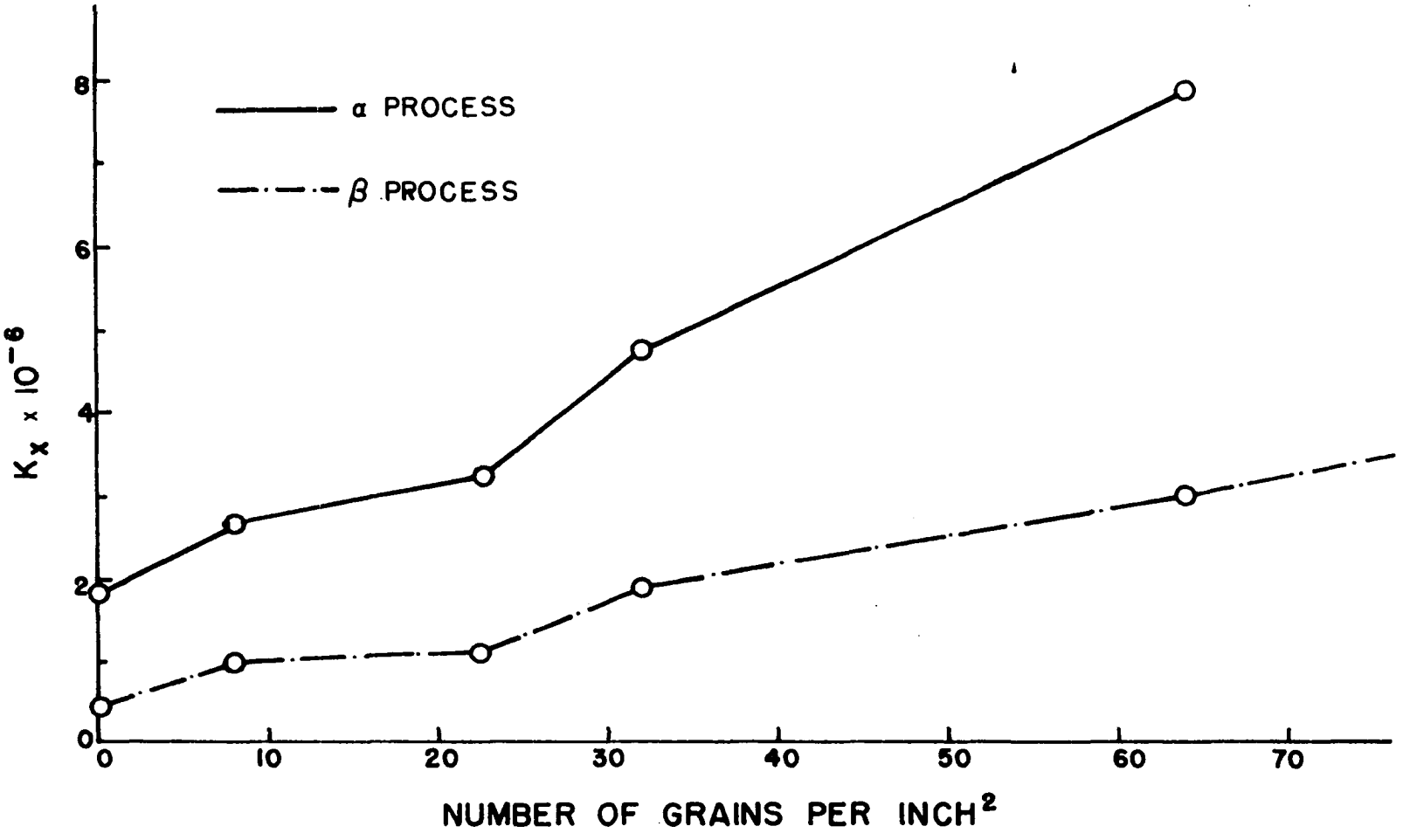

Figure 15. Experimental curves for the dependence of the annealing rates of α and β processes on the grain size

number of dislocation loops in the specimen as the grain size is made smaller. These dislocation loops make it harder for the defects to diffuse. The energy of interaction between point defects and randomly oriented dislocation loops is not known and therefore it is not possible to give a mathematical analysis.

The α-component definitely appears to be the contribution from the defects migrating to the grain boundaries, because of its pronounced dependence on the grain size. As to the nature of the β-component, a logical possibility is that it arises from the trapping of defects at the dislocation loops.

The gamma irradiation experiment was meant for investigating whether or not one of the two annealing processes was due to some kind of defects caused by the high gamma flux in the reactor. However the strength of the Cobalt-60 source used in this study was much smaller than what can be reasonably expected in the reactor. The damage from ionization caused by the gamma rays in the reactor irradiation will be very small because the size of the specimens used was small. The mechanism of defect production from gamma rays which could be of significance and which would be the most probable for gamma rays of average energy 2 to 3 MeV would be the damage caused by the Compton electrons.

These electrons might have sufficient energy to displace atoms as shown by Galavanov (35).

The threshold energy for displacement of a copper atom is known to be about 23 eV. Because of the similarity in the crystal structure between copper and bismuth we can assume this value to be true for bismuth also. The nucleus which scatters the Compton electron should receive at least 23 eV before it can get displaced. The maximum energy received by a Bi^{209} atom in a head-on-collision type elastic scattering with an electron is given by

$$E_{max} = \frac{2E}{1.95 \times 10^5} (E + 1.022) \qquad (26)$$

where E is the kinetic energy of the electron in MeV. In order to be able to give 23 eV to the bismuth atom, it is found that the Compton electron should have a kinetic energy of at least 1.11 MeV. The maximum energy E_m received by the electron in Compton scattering with a gamma ray of energy E_γ is given by

$$E_m = E_\gamma \left[1 - \frac{0.511}{E_\gamma + 0.511} \right] \qquad (27)$$

where all the energies are in MeV. From Equation 27, the minimum energy of the photon required to produce a Compton electron capable of transferring sufficient energy to a

bismuth atom so as to cause displacement is found to be 1.5 MeV, assuming that the maximum energy transfer occurs in the case of the Compton scattering and also in the case of the Bi^{209}-electron collision. This probably explains why no effect was observed in the gamma irradiation experiment using Cobalt-60 gamma rays of energies 1.17 MeV and 1.33 MeV.

In a qualitative evaluation of the damage due to the gamma rays in the reactor irradiation experiment, gammas from the following three sources have to be considered;

1. The prompt gammas from fission.
2. The photons emitted by fission products.
3. The photons resulting from the (n, γ) reaction in the aluminum cooling coils.

From the energy spectrum of the prompt fission gamma rays as given by Goldstein (36, p. 59), it can be seen that only about 10 per cent of the total number of photons/fission exceed 1.5 MeV in energy. According to Goldstein, the photon spectrum of the saturated fission products follows the same exponential energy dependence as the prompt gamma spectrum and their maximum energy is only 2.8 MeV (37, p. 34). The contribution of these gamma rays from fission products will be quite small in a low power reactor like the UTR-10. Therefore the only major contribution of gamma rays in the experiment could have been from the (n, γ) reactions in aluminum. Aluminum-27 has a thermal neutron (n, γ) cross section of

0.212 Fermis and gives off 0.77 photon per capture, in the energy interval 3 to 5 MeV, 0.21 photon per capture, within 5-7 MeV and 0.35 photon/capture at energy greater than 7 MeV. In order to investigate the effect of these gamma rays on the electrical resistivity of bismuth, high energy gamma sources are required.

The theoretical curve in Figure 2 indicates that if the attractive forces in the stress field around the grain boundaries were of a long range, the annealing rate should deviate rapidly from the linear dependence on the number of grain boundaries/inch^2. However, no such deviation is noticed in the experimental curves in Figure 15. This indicates that the nature of the stress field around large angle boundaries is quite different from that in the case of dislocation loops or low-angle grain boundaries which are known to exert attractive forces of long range on the mobile defects.

In the analysis of the recovery curves, it was assumed that the α-component at 12°C and at 40°C represented the same annealing process. However, the α-component at 12°C has a half life which is so small that almost all of that process should have been completed by the time the temperature was raised to 40°C and the annealing process corresponding to the α-component should not have been observed at 40°C. This means that the situation here is not completely

analogous to the case of radioactive decay of a mixture of two isotopes with different half lives. Perhaps there is an optimum temperature at which the number of defects taking part in a particular annealing process is a maximum. Such preferential annealing is known to take place at low temperatures (17). However, if that is the case here, it is not strictly valid to treat it as a simple diffusion problem. Diffusion could be one of the processes taking place, but the actual situation is more complex than simple diffusion and further work needs to be done to determine the mechanism of annealing.

VII. CONCLUSIONS

This study presents an investigation of the behavior of defects introduced by reactor irradiation in the presence of grain boundary type sinks, and has lead to the following conclusions about annealing in polycrystalline bismuth in the vicinity of room temperature.

1. The annealing rate of defects produced in polycrystalline bismuth by reactor irradiation is found to vary theoretically and experimentally as the inverse square of the average radius of the grains.

2. The stress field associated with the grain boundary sinks appears to have only little effect on the annealing rate of the defects.

3. Two different annealing components are observed for annealing of radiation damage in bismuth in the temperature range 12°C to 40°C.

4. Out of these two components, the short-lived component seems to be fairly definitely due to the grain boundary trapping and the long-lived component could be due to trapping of defects at the dislocation loops inside the grain which is known to increase in polycrystals as the grain size becomes smaller. However, further experimental evidence is required to support this.

5. The activation energies for the two components are

found to be nearly the same.

6. This method of investigating the effect of sinks on the annealing kinetics can be extended to other types of sinks also.

The conclusions stated above can not be checked with any experimental data since, to the knowledge of the author no such work has been done before.

VIII. SUGGESTIONS FOR FURTHER RESEARCH

Few quantitative studies have been made so far in investigating the consequences of thermal annealing of radiation induced defects produced at high temperatures (i.e., $T > 150^{\circ}K$). Such a defect state will have much greater mobility than at low temperatures and will be migrating to sinks or trapping centers. Under such conditions, the importance of interaction of defects with other atoms or with like-defects may be enhanced. Such studies of irradiated state are highly desirable and may help clarify our knowledge of the unirradiated state.

As stated in Section VII, the method used in this investigation may be extended to the study of trapping centers and sinks of various types other than the grain boundaries. For example, it is possible to create dislocations with preferred orientations by cold work and the migration of point defects to these dislocations can be studied through irradiation experiments of this kind yielding information about dislocation energies and their interaction with point defects.

It would be desirable in these studies to try to separate the neutron and the gamma effects in a mixed radiation field. The neutron effects may be separated by surrounding the samples with borated paraffin, although the reactivity loss might be a problem in the UTR-10.

It is also suggested that the neutron and gamma energy spectra in the radiation cavity of the UTR-10 be measured. The method of threshold detectors can be used for the neutron spectrum measurement. One way of measuring the gamma spectrum would be to use different types of glasses which have decolorization properties dependent on the energy of the photons they receive.

It would also be interesting to study the radiation damage due to thermal neutrons in light materials which are also good neutron absorbers. The recoil nucleus after the (n, γ) absorption in these materials is usually highly energetic and can give rise to significant radiation damage.

IX. ACKNOWLEDGEMENTS

The author wishes to express his sincere appreciation and gratitude for Dr. Glenn Murphy, Professor and head of the department of Nuclear Engineering at Iowa State University, for the valuable advice and help he received throughout the course of this research project. The kind consideration and magnanimity that Dr. Murphy and the Iowa State University have shown in financially assisting the author throughout the Ph. D. program shall never be forgotten.

Thanks are also due to Dr. Donald Glower, Sandia Corporation, New Mexico, for all the help and advice during the initial stages of this project.

The author also wishes to acknowledge the help of Dr. Abdul Rana, Professor of Nuclear Engineering, Iowa State University, who through many discussions aided the author in understanding the theoretical implications involved in this investigation.

X. LITERATURE CITED

1. Wigner, E. P. Theoretical Physics in the metallurgy laboratory of Chicago. Journal of Applied Physics 17:857-863. 1946.

2. Billington, D. S. Radiation effects in metals and alloys. In Harwood, J. J., Hausner, H. H., Morse, J. G. and Rauch, W. G., eds. The effects of radiation on materials. pp. 99-125. New York, New York, Reinhold Publishing Corporation. 1958.

3. Bohr, N. The penetration of atomic particles through matter. (Translated title) Kgl. Danske Videnskab. Selskab, Mat.-fys. Medd., 18: 8. 1948. Original not available for examination; cited in Dienes, G. J. and Vineyard, G. H. Radiation effects in solids. Interscience monographs in Physics and Astronomy. R. E. Marshak ed. New York, New York, Interscience Publishers Inc. 2: 7. 1957.

4. Seitz, F. On the disordering of solids by the action of fast massive particles. Discussions of Faraday Society 5: 271-282. 1949.

5. Brinkman, J. A. On the nature of radiation damage in metals. Journal of Applied Physics 25: 961-970. 1954.

6. _____. Production of atomic displacements by high energy particles. American Journal of Physics 24: 246-267. 1956.

7. Seitz, F. and Koehler, J. S. Displacement of atoms during irradiation. In Seitz, F. and Turnbull, D. eds. Solid State Physics. Vol. 2. pp. 307-442. New York, New York, Academic Press, Inc. 1956.

8. Dexter, D. L. Scattering of electrons from point singularities in metals. Physical Review 87: 768-777. 1952.

9. Jongenburger, P. The extra resistivity owing to vacancies in copper. Physical Review 90: 710-711. 1953.

10. _____. The extra resistivity due to vacancies in copper, silver and gold. Applied Scientific Research Series B, 3: 237-248. 1953.

11. _____. Extra resistivity due to interstitial atoms in copper. Nature 175: 545-546. 1955.

12. Blatt, F. J. Effect of point imperfections on the electrical properties of copper, I. Conductivity. Physical Review 99: 1708-1716. 1955.

13. Overhauser, A. W. and Gorman, R. L. Resistivity of interstitial atoms and vacancies in copper. Physical Review 102: 676-681. 1956.

14. Dienes, G. J. and Vineyard, G. H. Radiation effects in solids. In R. E. Marshak ed. Interscience Monographs in Physics and Astronomy. Vol. 2. New York, New York, Interscience Publishers Inc. 1957.

15. Billington, D. S. and Crawford, J. H., Jr. Radiation damage in solids. Princeton, New Jersey, Princeton University Press. 1961.

16. Radiation damage in solids. Proceedings of the symposium on radiation damage in solids and reactor materials. Vol. 1. Vienna, International Atomic Energy Agency. 1962.

17. Simmons, R. O., Koehler, J. S. and Baluffi, R. W. Present knowledge of point defects in irradiated Fcc metals. In the Proceedings of the Symposium on Radiation Damage in Solids and Reactor Materials. Vol. 1. pp. 155-204. Vienna, International Atomic Energy Agency. 1962.

18. Huntington, H. B. Self-consistent treatment of the vacancy mechanism for metallic diffusion. Physical Review 61: 325-338. 1942.

19. Brooks, H. Lattice vacancies and interstitials in metals. In the Proceedings of the Seminar on Impurities and Imperfections. pp. 1-27. Cleveland, Ohio, American Society for Metals. 1955.

20. Huntington, H. B. Mobility of interstitial atoms in a face-centered cubic metal. Physical Review 91: 1092-1098. 1953.

21. Fumi, H. G. Vacancies in monovalent metals. Philosophical Magazine 46: 1007-1020. 1955.

22. Gibson, J. B., Goland, A. N., Milgram, M. and Vineyard, G. H. Dynamics of radiation damage. Physical Review 120: 1229-1253. 1960.

23. Fletcher, R. C. and Brown, W. L. Annealing of bombardment damage in germanium. Physical Review 91: 237. 1953.

24. Letaw, H., Jr. Thermal acceptors in germanium. Journal of Physics and Chemistry of Solids 1: 100-116. 1956.

25. Conference on radiation effects in semiconductors. Journal of Applied Physics 30: 1117-1316. 1959.

26. Overhauser, A. W. Isothermal annealing effects in irradiated copper. Physical Review 90: 393-400. 1953.

27. Glower, D. D. Effect of irradiation on the electrical conductivity in bismuth. Unpublished Ph. D. thesis. Ames, Iowa, Library, Iowa State University of Science and Technology. 1960.

28. Bartlett, J. H. and Dienes, G. J. Combined pairs of vacancies in copper. Physical Review 89: 848-850. 1953.

29. Webb, W. W. The interaction of solutes with dislocation walls. Acta Metallurgica 5: 89-96. 1957.

30. Cottrell, A. H. and Bilby, B. A. Dislocation theory of yielding and strain ageing of iron. Physical Society of London. Proceedings Series A, 62: 49-62. 1949.

31. McLean, D. Grain boundaries in metals. Oxford, Clarendon Press. 1957.

32. Carslaw, H. S. The cooling of a solid sphere with a concentric core of a different material. Cambridge Philosophical Society, Proceedings 20: 399-410. 1921.

33. Van Bueren, H. G. Imperfections in crystals. Amsterdam, North-Holland Publishing Company. 1960.

34. American Society for Testing Materials. Tentative methods for estimating the average grain size of non-ferrous metals, other than copper and their alloys. In ASTM Standards 1955. pp. 1390-1395. Part 2. Non-Ferrous Metals. Author, Philadelphia, Pennsylvania. c1955.

35. Galavanov, V. V. Displacement of atoms in a solid by the action of gamma rays. Soviet Physics-Solid State 1: 390-399. 1959.

36. Goldstein, H. Fundamental aspects of reactor shielding. Reading, Massachusetts, Addison-Wesley Publishing Co., Inc. 1959.

37. Rockwell, III., T. Reactor shielding design manual. Princeton, New Jersey, D. Van Nostrand Company, Inc. 1956.

XI. APPENDIX

Table 2. Electrical resistivity data for specimen A ($\frac{\text{Area of cross-section}}{\text{Length}}$ = 0.0218379 cm)

Time (minutes)	Potential drop across specimen (μV)	Current (mA)	Resistivity ($\mu\Omega$-cm)	Normalized resistivity ($\mu\Omega$-cm)	$\Delta\rho$ ($\mu\Omega$-cm)
0	466.0	81.36	125.01	122.35	0
3	466.5	81.88	124.42	122.35	0
7	467.0	81.88	124.55	122.57	0.22
17	468.5	81.97	124.81	122.87	0.52
22	468.5	82.06	124.73	122.83	0.48
28	469.0	82.06	124.78	122.98	0.63
41	470.0	82.24	124.82	123.42	1.07
47	468.5	82.15	124.50	123.39	1.04
53	468.5	82.24	124.41	123.60	1.25
57	468.0	82.24	124.31	123.73	1.38
76	468.5	82.24	124.35	124.05	1.70
86	467.0	82.06	124.32	124.05	1.70
92	467.0	82.06	124.36	124.27	1.92
105	467.5	82.15	124.27	124.27	1.92
114	468.0	82.15	124.50	124.50	2.15
120	468.5	82.15	124.56	124.56	2.21
123	468.0	82.15	124.50	124.50	2.15
134	470.0	82.32	124.67	124.67	2.32
139	469.5	82.24	124.72	124.72	2.37
144	469.5	82.24	124.67	124.67	2.32
155	470.0	82.15	124.87	124.87	2.52
168	470.5	82.24	124.94	124.94	2.59
173	471.0	82.32	125.05	125.05	2.70
179	471.5	82.27	125.09	125.09	2.74
217	473.5	82.59	125.17	125.17	2.82
226	473.5	82.59	125.23	125.23	2.88
232	475.3	82.76	125.43	125.31	2.96
258	475.5	82.67	125.65	125.40	3.05
268	475.0	82.67	125.40	125.40	3.05
296	473.5	82.67	125.06	125.47	3.12
304	473.0	82.76	125.02	125.52	3.17
316	473.0	82.76	125.02	125.52	3.17
338	472.0	82.76	124.72	125.48	3.13
352	473.5	82.85	124.77	125.53	3.18
362	473.0	82.76	124.88	125.53	3.18
378	474.0	82.76	125.10	125.55	3.20
389	474.0	82.80	125.05	125.45	3.10

Table 2. (Continued)

Time (minutes)	Potential drop across specimen (μV)	Current (mA)	Resistivity ($\mu\Omega$-cm)	Normalized resistivity ($\mu\Omega$-cm)	$\Delta\rho$ ($\mu\Omega$-cm)
414	475.0	82.76	125.40	125.50	3.15
443	475.5	82.76	125.45	125.45	3.10
452	475.5	82.76	125.52	125.52	3.17
458	476.0	82.85	125.50	125.50	3.15
480	476.5	82.88	125.61	125.50	3.15
505	477.0	82.85	125.69	125.53	3.18
522	478.0	82.94	125.92	125.47	3.12
540	478.5	82.94	125.95	125.50	3.15
565	479.0	83.11	125.90	125.45	3.10
570	479.5	83.11	126.00	125.55	3.20
593	479.5	83.11	125.95	125.50	3.15
600	478.0	83.06	125.74	125.40	3.05
607	478.5	83.20	125.60	125.33	2.98
615	479.0	83.29	125.60	125.37	3.02
620	478.5	83.29	125.50	125.27	2.92
627	478.5	83.20	125.55	125.20	2.85
640	479.0	83.29	125.55	125.20	2.85
658	476.0	83.11	125.11	125.11	2.76
668	476.0	83.11	125.14	125.03	2.68
690	475.5	83.38	124.52	124.97	2.62
700	476.0	83.47	124.46	125.00	2.65
725	474.0	83.47	124.05	124.95	2.60
747	474.0	83.47	123.94	124.93	2.58
770	473.5	83.38	124.01	124.91	2.56
780	474.0	83.47	123.95	124.92	2.57
790	473.0	83.47	123.77	124.90	2.55
810	472.5	83.38	123.72	124.85	2.50
825	476.0	83.47	124.52	124.90	2.55
835	475.0	83.38	124.46	124.78	2.43
845	473.0	83.47	123.78	124.85	2.50
855	473.0	83.47	123.71	124.88	2.53
870	473.0	83.47	123.68	124.80	2.45
885	472.0	83.38	123.60	124.82	2.47
895	472.0	83.38	123.65	124.78	2.43
905	473.0	83.38	123.86	124.81	2.46
915	473.5	83.47	123.90	124.80	2.45
930	474.0	83.55	123.94	124.75	2.40
946	474.5	83.55	124.03	124.80	2.45
955	475.0	83.55	124.14	124.77	2.42

Table 2. (Continued)

Time (minutes)	Potential drop across specimen (μV)	Current (mA)	Resistivity ($\mu\Omega$-cm)	Normalized resistivity ($\mu\Omega$-cm)	$\Delta\rho$ ($\mu\Omega$-cm)
968	475.0	83.47	124.22	124.75	2.40
980	475.0	83.47	124.30	124.70	2.35
997	476.5	83.73	124.32	124.68	2.33
1005	475.0	83.64	123.98	124.75	2.40
1017	478.0	83.68	124.75	124.75	2.40
1030	479.0	83.64	125.01	124.74	2.39
1045	478.5	83.55	125.07	124.67	2.32
1050	479.0	83.55	125.15	124.70	2.35
1100	522.5	83.47	136.65	124.05	1.70
1104	522.0	83.55	136.37	123.77	1.42
1113	522.5	83.55	136.55	123.70	1.35
1119	522.0	83.47	136.60	123.55	1.20
1127	521.0	83.47	136.27	123.35	1.00
1135	520.5	83.47	136.16	123.34	0.99
1150	519.0	83.38	135.93	123.10	0.75
1170	520.0	83.47	135.98	123.05	0.70
1175	519.5	83.47	135.89	122.97	0.62
1184	519.0	83.47	135.80	122.97	0.62
1195	519.0	83.47	135.75	122.90	0.55
1205	519.0	83.47	135.84	122.92	0.57
1215	522.0	83.55	136.35	122.90	0.55
1225	521.5	83.47	136.42	122.87	0.52
1235	520.0	83.47	136.10	122.90	0.55
1243	519.0	83.38	135.94	122.80	0.45
1253	521.5	83.38	136.56	122.82	0.47
1264	519.5	83.64	135.63	122.87	0.52
1270	519.0	83.64	135.54	122.80	0.45
1286	519.0	83.64	135.55	122.86	0.51
1295	518.0	83.47	135.58	122.77	0.42
1302	519.5	83.64	135.61	122.81	0.46
1325	519.0	83.47	135.77	122.81	0.46
1355	518.0	83.55	135.36	122.76	0.41
1360	518.5	83.55	135.41	122.81	0.46
1370	518.5	83.64	135.33	122.73	0.38
1380	523.0	83.64	136.57	122.70	0.35
1395	520.0	83.64	135.74	122.78	0.43
1405	520.0	83.82	135.55	122.77	0.42
1428	520.0	83.73	135.56	122.69	0.34

Table 2. (Continued)

Time (minutes)	Potential drop across specimen (μ V)	Current (mA)	Resistivity ($\mu\Omega$-cm)	Normalized resistivity ($\mu\Omega$-cm)	$\Delta\rho$ ($\mu\Omega$-cm)
1433	520.0	83.73	135.63	122.76	0.41
1445	519.5	83.73	135.45	122.77	0.42
1462	520.0	83.82	135.63	122.76	0.41
1482	520.0	83.82	135.42	122.74	0.39
1491	520.0	83.82	135.45	122.76	0.41
1510	521.5	83.90	135.81	122.76	0.41
1520	521.5	83.90	135.77	122.77	0.42
1530	519.0	83.64	135.53	122.76	0.41
1545	519.0	83.82	135.35	122.75	0.40

Table 3. Electrical resistivity data for specimen B ($\frac{\text{Area of cross-section}}{\text{Length}}$ = 0.017896 cm)

Time (minutes)	Potential drop across specimen (μV)	Current (mA)	Resistivity ($\mu\Omega$-cm)	Normalized resistivity ($\mu\Omega$-cm)	$\Delta\rho$ ($\mu\Omega$-cm)
0	583.5	81.36	128.35	126.05	0
5	583.5	81.36	128.31	126.06	0.01
20	588.5	82.06	128.33	126.35	0.30
35	589.0	82.24	128.11	126.45	0.40
47	586.5	82.15	127.72	126.70	0.65
58	584.0	82.15	127.28	126.75	0.70
74	585.0	82.24	127.24	126.92	0.87
78	585.0	82.15	127.38	127.06	1.01
85	584.0	82.06	127.40	127.12	1.07
91	583.5	82.06	127.26	127.14	1.09
97	584.0	82.15	127.28	127.28	1.23
105	585.0	82.15	127.45	127.45	1.40
115	585.0	82.15	127.45	127.45	1.40
122	585.5	82.15	127.54	127.54	1.49
135	587.5	82.32	127.70	127.70	1.65
155	587.0	82.15	127.86	127.86	1.81
167	588.0	82.24	127.90	127.90	1.85
172	589.0	82.32	128.10	128.10	2.05
185	589.5	82.32	128.12	128.12	2.07
210	592.0	82.59	128.22	128.22	2.17
215	592.0	82.59	128.32	128.32	2.27
235	594.0	82.76	128.45	128.45	2.40
247	594.5	82.67	128.72	128.40	2.35
256	595.0	82.67	128.80	128.52	2.47
264	595.5	82.67	128.87	128.62	2.57
278	593.5	82.59	128.59	128.59	2.54
304	593.0	82.76	128.24	128.75	2.70
310	593.0	82.76	128.17	128.68	2.63
330	593.0	82.76	128.22	128.80	2.75
346	592.0	82.76	128.03	128.81	2.76
370	593.7	82.76	128.38	128.84	2.79
390	594.5	82.80	128.53	128.90	2.85
411	595.5	82.80	128.70	128.88	2.83
424	597.0	82.85	128.96	128.96	2.91
435	597.0	82.94	128.87	128.87	2.82
445	597.0	82.85	128.94	128.94	2.89
465	597.0	82.85	128.96	128.96	2.91

Table 3. (Continued)

Time (minutes)	Potential drop across specimen (μ V)	Current (mA)	Resistivity ($\mu\Omega$-cm)	Normalized resistivity ($\mu\Omega$-cm)	$\Delta\rho$ ($\mu\Omega$-cm)
477	597.5	82.89	129.02	128.92	2.87
513	598.0	82.89	129.11	128.91	2.86
551	601.0	83.03	129.46	129.00	2.95
565	601.0	83.11	129.39	128.93	2.88
587	601.0	83.03	129.44	128.98	2.93
593	601.0	83.11	129.44	128.98	2.93
598	600.0	83.06	129.29	128.94	2.89
603	599.5	83.20	129.00	128.72	2.77
610	599.5	83.29	128.78	128.55	2.50
623	599.0	83.29	128.69	128.46	2.41
640	598.0	83.29	128.53	128.35	2.30
657	596.5	83.11	128.43	128.29	2.24
668	596.0	83.11	128.28	128.28	2.23
687	595.5	83.29	127.98	128.24	2.19
695	596.0	83.47	127.76	128.16	2.11
710	594.5	83.38	127.62	128.17	2.12
722	594.5	83.55	127.31	128.16	2.11
728	594.5	83.64	127.17	128.09	2.04
748	594.0	83.64	127.10	128.07	2.02
760	592.5	83.38	127.15	128.02	1.97
774	592.0	83.38	127.11	128.03	1.98
785	592.5	83.47	126.99	127.96	1.91
797	592.5	83.47	127.00	128.01	1.96
812	592.5	83.47	127.02	128.03	1.98
836	593.0	83.47	127.18	128.01	1.96
852	592.0	83.47	126.90	128.00	1.95
860	590.5	83.29	126.85	127.95	1.90
878	591.0	83.47	126.76	127.96	1.91
890	590.5	83.38	126.72	127.90	1.85
895	591.0	83.38	126.86	128.01	1.96
906	592.5	83.47	127.04	128.01	1.96
915	592.5	83.47	127.04	127.96	1.91
925	593.0	83.47	127.15	128.00	1.95
940	593.5	83.47	127.24	127.99	1.94
955	594.5	83.47	127.42	127.97	1.92
963	595.0	83.55	127.41	127.96	1.91
990	596.5	83.64	127.63	127.95	1.90
1005	597.5	83.73	127.70	127.98	1.93
1020	598.5	83.73	127.95	127.95	1.90

Table 3. (Continued)

Time (minutes)	Potential drop across specimen (μV)	Current (mA)	Resistivity ($\mu\Omega$-cm)	Normalized resistivity ($\mu\Omega$-cm)	$\Delta\rho$ ($\mu\Omega$-cm)
1036	599.5	83.64	128.29	127.97	1.92
1052	599.5	83.64	128.31	127.95	1.90
1100	653.5	83.47	140.08	127.60	1.55
1103	653.5	83.55	139.99	127.41	1.36
1106	653.5	83.55	139.94	127.30	1.25
1115	653.0	83.47	139.98	127.30	1.25
1120	653.5	83.47	140.12	127.18	1.13
1127	652.5	83.47	139.92	127.12	1.07
1145	652.5	83.47	139.93	126.99	0.94
1159	652.0	83.55	139.71	126.95	0.90
1170	652.5	83.55	139.72	126.84	0.79
1178	652.5	83.55	139.76	126.82	0.77
1188	655.5	83.47	140.52	126.85	0.80
1194	651.0	83.47	139.55	126.77	0.72
1209	651.5	83.47	139.68	126.74	0.69
1225	654.0	83.55	140.11	126.66	0.61
1243	651.5	83.47	139.71	126.68	0.63
1250	649.0	83.47	139.12	126.60	0.55
1258	650.0	83.55	139.27	126.65	0.60
1268	651.0	83.64	139.27	126.65	0.60
1280	652.0	83.64	139.51	126.58	0.53
1294	649.5	83.47	139.21	126.55	0.50
1310	651.0	83.64	139.25	126.57	0.52
1334	651.0	83.55	139.49	126.55	0.50
1350	649.5	83.64	138.98	126.50	0.45
1365	649.5	83.64	138.94	126.46	0.41
1374	650.0	83.64	139.05	126.43	0.38
1378	651.0	83.64	139.30	126.54	0.49
1410	651.0	83.64	139.23	126.52	0.47
1425	651.5	83.73	139.28	126.54	0.49
1435	652.0	83.82	139.25	126.55	0.50
1440	652.0	83.82	139.16	126.50	0.45
1460	652.0	83.82	139.22	126.47	0.42
1466	651.5	83.82	139.06	126.40	0.35
1480	651.0	83.82	139.01	126.45	0.40
1486	651.5	83.82	139.06	126.48	0.43
1509	653.5	83.90	139.37	126.48	0.43
1525	653.0	83.82	139.36	126.47	0.42
1541	651.5	83.82	139.12	126.54	0.49
1552	652.0	83.90	139.03	126.51	0.46

Table 4. Electrical resistivity data for specimen C ($\frac{\text{Area of cross-section}}{\text{Length}}$ = 0.0191146 cm)

Time (minutes)	Potential drop across specimen (μV)	Current (mA)	Resistivity ($\mu\Omega$-cm)	Normalized resistivity ($\mu\Omega$-cm)	$\Delta\rho$ ($\mu\Omega$-cm)
0	527.8	81.36	124.01	122.00	0
12	531.5	81.90	124.01	122.15	0.15
25	532.0	82.06	123.93	122.25	0.25
45	532.5	82.15	123.93	122.82	0.82
57	531.5	82.24	123.56	122.96	0.96
72	530.5	82.15	123.43	123.12	1.12
90	529.5	82.06	123.37	123.25	1.25
110	531.5	82.24	123.51	123.51	1.51
120	531.0	82.15	123.50	123.50	1.50
130	532.0	82.24	123.65	123.65	1.65
135	532.5	82.24	123.77	123.77	1.77
150	532.5	82.24	123.82	123.82	1.82
156	532.5	82.15	123.91	123.91	1.91
177	534.0	82.32	123.95	123.95	1.95
185	534.5	82.32	124.06	124.06	2.06
192	534.0	82.32	124.00	124.00	2.00
200	536.5	82.59	124.16	124.16	2.16
212	537.0	82.59	124.28	124.28	2.28
215	536.5	82.59	124.20	124.20	2.20
223	536.5	82.59	124.22	124.22	2.22
232	537.5	82.59	124.35	124.35	2.35
247	539.5	82.67	124.74	124.49	2.49
255	540.0	82.76	124.69	124.44	2.44
260	540.0	82.76	124.69	124.56	2.56
270	539.5	82.67	124.76	124.55	2.55
274	539.5	82.67	124.70	124.70	2.70
285	538.0	82.59	124.52	124.60	2.60
290	538.0	82.59	124.53	124.72	2.72
298	537.5	82.67	124.28	124.65	2.65
320	538.0	82.76	124.30	124.75	2.75
330	538.5	82.76	124.37	124.88	2.88
338	538.0	82.76	124.26	124.96	2.96
346	538.0	82.76	124.21	124.91	2.91
365	539.5	82.76	124.60	125.01	3.01
370	539.5	82.76	124.61	125.02	3.02
380	539.5	82.76	124.61	125.02	3.02
389	540.0	82.80	124.67	125.00	3.00

Table 4. (Continued)

Time (minutes)	Potential drop across specimen (μV)	Current (mA)	Resistivity ($\mu\Omega$-cm)	Normalized resistivity ($\mu\Omega$-cm)	$\Delta\rho$ ($\mu\Omega$-cm)
404	541.0	82.80	124.91	125.11	3.11
418	541.5	82.80	124.97	125.05	3.05
446	542.0	82.85	125.02	125.02	3.02
457	542.5	82.85	125.15	125.15	3.15
465	542.0	82.85	125.10	125.10	3.10
476	543.0	82.89	125.26	125.18	3.18
484	543.0	82.89	125.24	125.14	3.14
492	543.5	82.94	125.22	125.10	3.10
535	544.0	82.94	125.32	125.20	3.20
542	543.5	82.94	125.21	125.09	3.09
575	544.5	83.11	125.25	125.09	3.09
580	545.5	83.03	125.55	125.14	3.14
593	545.5	83.11	125.42	125.11	3.11
601	544.5	83.06	125.32	125.01	3.01
612	545.5	83.29	125.15	124.94	2.94
619	545.0	83.29	125.07	124.86	2.86
630	544.0	83.20	125.03	124.82	2.82
635	543.5	83.20	124.89	124.73	2.73
640	544.0	83.29	124.90	124.74	2.74
651	543.0	83.11	124.88	124.76	2.76
659	544.0	83.29	124.79	124.67	2.67
664	542.5	83.20	124.62	124.70	2.70
681	542.0	83.29	124.44	124.66	2.66
690	541.5	83.38	124.15	124.56	2.56
697	542.5	83.47	124.19	124.60	2.60
713	541.5	83.38	124.09	124.62	2.62
732	542.5	83.64	123.94	124.60	2.60
738	542.0	83.64	123.84	124.50	2.50
743	541.5	83.64	123.72	124.54	2.54
765	540.0	83.38	123.85	124.55	2.55
770	539.5	83.38	123.72	124.42	2.42
784	540.5	83.47	123.82	124.52	2.52
790	540.5	83.55	123.68	124.50	2.50
800	540.0	83.47	123.63	124.45	2.45
825	541.0	83.47	123.86	124.52	2.52
842	540.5	83.47	123.79	124.45	2.45
850	540.5	83.47	123.77	124.53	2.53
860	540.0	83.47	123.61	124.43	2.43
871	539.5	83.47	123.59	124.45	2.45

Table 4. (Continued)

Time (minutes)	Potential drop across specimen (μV)	Current (mA)	Resistivity ($\mu\Omega$-cm)	Normalized resistivity ($\mu\Omega$-cm)	$\Delta\rho$ ($\mu\Omega$-cm)
875	539.5	83.47	123.50	124.36	2.36
890	539.0	83.38	123.62	124.48	2.48
900	539.0	83.38	123.62	124.40	2.40
912	541.0	83.55	123.78	124.48	2.48
924	541.0	83.55	123.78	124.44	2.44
935	540.5	83.47	123.76	124.42	2.42
951	541.0	83.47	123.93	124.50	2.50
962	541.5	83.55	123.91	124.40	2.40
968	542.5	83.64	123.93	124.42	2.42
985	542.0	83.47	124.16	124.49	2.49
992	543.5	83.64	124.16	124.45	2.45
1000	543.5	83.73	124.13	124.42	2.42
1012	544.0	83.73	124.18	124.39	2.39
1020	545.5	83.73	124.48	124.48	2.48
1036	545.5	83.64	124.70	124.41	2.41
1044	546.0	83.64	124.81	124.45	2.45
1050	546.0	83.64	124.79	124.38	2.38
1100	591.0	83.47	135.32	124.05	2.05
1108	591.5	83.55	135.33	123.71	1.71
1114	591.0	83.47	135.32	123.56	1.56
1120	591.0	83.47	135.33	123.44	1.44
1131	591.5	83.47	135.40	123.36	1.36
1149	589.5	83.47	135.02	123.33	1.33
1156	589.0	83.47	134.89	123.18	1.18
1166	590.0	83.55	135.02	123.21	1.21
1175	590.5	83.55	135.09	123.20	1.20
1192	588.5	83.47	134.80	123.10	1.10
1205	590.0	83.47	135.09	123.12	1.12
1215	590.5	83.47	135.19	123.13	1.13
1225	590.5	83.55	135.15	123.10	1.10
1240	590.0	83.47	135.10	123.13	1.13
1248	589.0	83.47	134.93	123.08	1.08
1275	590.0	83.73	134.69	123.09	1.09
1285	589.0	83.64	134.61	123.05	1.05
1293	588.0	83.47	134.70	123.06	1.06
1302	589.5	83.64	134.74	123.08	1.08
1334	590.0	83.55	134.95	123.06	1.06
1347	589.5	83.64	134.71	123.00	1.00

Table 4. (Continued)

Time (minutes)	Potential drop across specimen (μV)	Current (mA)	Resistivity ($\mu\Omega$-cm)	Normalized resistivity ($\mu\Omega$-cm)	$\Delta\rho$ ($\mu\Omega$-cm)
1355	589.0	83.64	134.66	123.06	1.06
1365	589.0	83.64	134.58	123.10	1.10
1371	590.5	83.64	135.00	122.99	0.99
1380	592.0	83.64	135.25	123.11	1.11
1388	591.5	83.64	135.16	123.02	1.02
1395	590.0	83.64	134.86	123.05	1.05
1430	593.0	83.82	135.26	123.12	1.12
1442	592.5	83.82	135.13	123.08	1.08
1452	592.5	83.82	135.13	123.08	1.08
1465	593.5	83.99	135.05	123.10	1.10
1470	593.5	83.99	135.10	123.05	1.05
1480	592.5	83.82	135.13	123.08	1.08
1483	592.0	83.82	135.05	123.00	1.00
1492	593.0	83.90	134.96	122.98	0.98
1508	592.5	83.90	134.86	123.01	1.01
1530	592.0	83.73	135.10	122.96	0.96
1537	592.0	83.82	135.03	123.05	1.05
1548	592.0	83.82	134.98	123.03	1.03

Table 5. Electrical resistivity data for specimen D ($\frac{\text{Area of cross-section}}{\text{Length}}$ = 0.0185152 cm)

Time (minutes)	Potential drop across specimen (μV)	Current (mA)	Resistivity ($\mu\Omega$-cm)	Normalized resistivity ($\mu\Omega$-cm)	$\Delta\rho$ ($\mu\Omega$-cm)
0	547.5	81.36	124.61	122.60	0.00
10	552.0	81.88	124.85	122.96	0.36
15	552.0	81.97	124.72	122.92	0.32
25	553.5	82.06	124.88	123.17	0.57
40	553.5	82.24	124.62	123.30	0.70
50	552.0	82.15	124.60	123.45	0.85
54	552.0	82.24	124.42	123.60	1.00
61	551.0	82.24	124.07	123.66	1.06
72	550.0	82.15	123.96	123.66	1.06
78	550.5	82.15	124.04	123.75	1.15
89	550.0	82.06	124.07	123.95	1.35
100	551.5	82.24	124.16	124.11	1.51
118	550.5	82.15	124.11	124.11	1.51
130	551.50	82.24	124.20	124.20	1.60
144	552.5	82.24	124.39	124.39	1.79
154	554.5	82.15	124.95	124.45	1.85
172	555.0	82.24	124.95	124.45	1.85
183	553.5	82.24	124.61	124.58	1.98
202	554.0	82.32	124.59	124.59	1.99
216	556.0	82.59	124.68	124.68	2.08
230	556.0	82.59	124.66	124.66	2.06
245	558.5	82.67	125.23	124.77	2.17
252	558.0	82.67	125.02	124.75	2.15
272	558.5	82.67	125.04	124.85	2.25
296	557.5	82.67	124.91	124.91	2.31
305	557.0	82.76	124.63	124.85	2.25
320	556.5	82.76	124.46	124.91	2.31
327	556.5	82.76	124.65	124.96	2.36
340	555.5	82.76	124.24	124.94	2.34
352	556.0	82.76	124.37	125.00	2.40
372	556.5	82.76	124.55	124.96	2.36
390	557.0	82.80	124.55	124.98	2.38
396	557.5	82.80	124.65	124.93	2.33
418	558.5	82.76	124.93	124.95	2.35
423	559.5	82.85	124.99	124.99	2.39
436	559.5	82.94	125.00	125.00	2.40
440	559.0	82.85	124.92	124.92	2.32

Table 5. (Continued)

Time (minutes)	Potential drop across specimen (μV)	Current (mA)	Resistivity ($\mu\Omega$-cm)	Normalized resistivity ($\mu\Omega$-cm)	$\Delta\rho$ ($\mu\Omega$-cm)
456	559.0	82.80	125.04	125.04	2.44
471	559.0	82.85	124.93	124.97	2.37
485	559.0	82.89	124.92	125.02	2.42
508	559.5	82.85	125.02	124.97	2.37
512	560.0	82.89	125.14	125.02	2.42
539	560.0	82.94	125.09	125.02	2.42
545	561.0	82.94	125.36	124.96	2.36
556	562.0	83.03	125.34	124.94	2.34
563	563.0	83.11	125.45	124.95	2.35
567	563.0	83.11	125.45	125.05	2.45
580	562.5	83.03	125.41	124.96	2.36
588	562.5	83.03	125.40	125.00	2.40
593	563.0	83.11	125.43	125.03	2.43
600	561.5	83.06	125.21	124.91	2.31
610	562.5	83.29	125.07	124.87	2.27
617	562.0	83.29	124.97	124.77	2.17
635	561.0	83.20	124.87	124.67	2.07
647	561.0	83.29	124.74	124.62	2.02
659	561.0	83.29	124.73	124.61	2.01
668	560.0	83.29	124.68	124.64	2.04
673	561.0	83.38	124.55	124.55	1.95
685	559.0	83.29	124.31	124.55	1.95
690	559.0	83.38	124.08	124.48	1.88
709	558.5	83.38	124.02	124.54	1.94
715	559.0	83.47	124.01	124.45	1.85
740	558.5	83.64	123.62	124.42	1.82
765	556.5	83.38	123.60	124.40	1.80
778	556.5	83.38	123.58	124.42	1.82
798	557.5	83.55	123.53	124.41	1.81
805	556.5	83.47	123.46	124.38	1.78
825	557.5	83.47	123.66	124.34	1.74
847	556.5	83.47	123.42	124.30	1.70
861	555.0	83.29	123.40	124.35	1.75
868	556.5	83.47	123.43	124.35	1.75
875	557.0	83.47	123.52	124.32	1.72
883	557.0	83.47	123.51	124.31	1.71
890	557.0	83.47	123.51	124.31	1.71
896	556.0	83.38	123.47	124.27	1.67
914	557.5	83.55	123.52	124.32	1.72

Table 5. (Continued)

Time (minutes)	Potential drop across specimen (μV)	Current (mA)	Resistivity ($\mu\Omega$-cm)	Normalized resistivity ($\mu\Omega$-cm)	$\Delta\rho$ ($\mu\Omega$-cm)
920	557.5	83.55	123.50	124.26	1.66
925	557.5	83.47	123.63	124.35	1.75
930	557.0	83.47	123.58	124.30	1.70
945	558.0	83.55	123.65	124.33	1.73
967	559.5	83.64	123.83	124.31	1.71
983	559.0	83.47	124.02	124.34	1.74
1005	561.0	83.73	124.03	124.27	1.67
1030	562.5	83.64	124.53	124.31	1.71
1035	562.5	83.64	124.54	124.30	1.70
1050	563.0	83.64	124.65	124.25	1.65
1103	609.5	83.47	135.20	124.00	1.40
1105	611.0	83.55	135.41	123.81	1.21
1110	610.0	83.55	135.21	123.72	1.12
1116	609.0	83.47	135.10	123.60	1.00
1125	610.0	83.55	135.14	123.56	0.96
1134	608.5	83.47	134.95	123.55	0.95
1139	607.5	83.47	134.76	123.42	0.82
1150	608.5	83.47	134.77	123.41	0.81
1165	608.5	83.55	134.88	123.36	0.76
1172	607.5	83.47	134.73	123.25	0.65
1184	607.0	83.47	134.68	123.28	0.68
1195	607.5	83.47	134.72	123.28	0.68
1202	607.0	83.47	134.65	123.17	0.57
1212	609.5	83.55	135.09	123.25	0.65
1220	609.0	83.55	134.98	123.18	0.58
1225	610.0	83.55	135.22	123.18	0.58
1249	607.5	83.47	134.75	123.19	0.59
1256	607.0	83.55	134.48	123.12	0.52
1271	608.0	83.64	134.63	123.13	0.53
1284	608.0	83.64	134.59	123.19	0.59
1292	606.0	83.47	134.45	123.09	0.49
1300	607.5	83.64	134.51	123.11	0.51
1314	607.5	83.64	134.48	123.08	0.48
1325	607.5	83.55	134.62	123.10	0.50
1344	607.5	83.64	134.51	123.11	0.51
1365	607.0	83.64	134.38	123.14	0.54
1380	608.0	83.64	134.54	123.10	0.50
1387	607.5	83.64	134.49	123.05	0.45

Table 5. (Continued)

Time (minutes)	Potential drop across specimen (μV)	Current (mA)	Resistivity ($\mu\Omega$-cm)	Normalized resistivity ($\mu\Omega$-cm)	$\Delta\rho$ ($\mu\Omega$-cm)
1410	607.0	83.64	134.41	123.01	0.41
1417	608.0	83.73	134.50	123.10	0.50
1434	609.0	83.82	134.57	123.07	0.47
1463	609.0	83.82	134.53	123.09	0.49
1472	608.5	83.82	134.44	123.12	0.52
1480	608.5	83.82	134.45	123.09	0.49
1498	609.0	83.90	134.38	123.10	0.50
1514	610.0	83.90	134.59	123.04	0.44
1522	609.0	83.73	134.65	123.09	0.49
1548	608.0	83.82	134.32	123.07	0.47

Table 6. Electrical resistivity data for specimen E ($\frac{\text{Area of cross-section}}{\text{Length}}$ = 0.0202562 cm)

Time (minutes)	Potential drop across specimen (μV)	Current (mA)	Resistivity ($\mu\Omega$-cm)	Normalized resistivity ($\mu\Omega$-cm)	$\Delta\rho$ ($\mu\Omega$-cm)
0	504.0	81.36	125.47	123.07	0.07
5	504.5	81.36	125.65	123.40	0.40
10	507.5	81.88	125.59	123.47	0.47
17	508.5	81.97	125.65	123.65	0.65
23	509.0	82.06	125.65	123.72	0.72
27	509.5	82.06	125.73	123.88	0.88
35	509.5	82.24	125.55	123.90	0.90
39	509.0	82.24	125.42	123.99	0.99
46	508.0	82.15	125.30	124.06	1.06
49	508.0	82.15	125.29	124.28	1.28
60	506.5	82.24	124.77	124.31	1.31
64	506.5	82.24	124.77	124.40	1.40
75	506.5	82.24	124.76	124.44	1.44
85	505.5	82.06	124.78	124.50	1.50
95	506.0	82.15	124.71	124.66	1.66
100	506.0	82.15	124.76	124.76	1.76
109	506.5	82.24	124.75	124.75	1.75
115	506.0	82.15	124.82	124.82	1.82
125	507.5	82.24	124.97	124.97	1.97
137	507.5	82.24	125.00	125.00	2.00
142	508.0	82.24	125.14	125.14	2.14
165	509.0	82.32	125.21	125.21	2.21
175	509.0	82.32	125.29	125.29	2.29
183	509.0	82.24	125.40	125.40	2.40
194	509.5	82.32	125.38	125.38	2.38
202	511.5	82.59	125.48	125.48	2.48
211	512.0	82.59	125.55	125.55	2.55
216	511.5	82.59	125.50	125.50	2.50
233	512.0	82.59	125.62	125.57	2.57
239	514.0	82.76	125.80	125.66	2.66
250	514.0	82.67	125.94	125.64	2.64
263	514.5	82.76	125.98	125.72	2.72
275	512.5	82.59	125.73	125.68	2.68
282	513.0	82.59	125.77	125.77	2.77
300	511.5	82.67	125.39	125.85	2.85
308	512.0	82.76	125.29	125.80	2.80
320	512.0	82.76	125.35	125.86	2.86

Table 6. (Continued)

Time (minutes)	Potential drop across specimen (μV)	Current (mA)	Resistivity ($\mu\Omega$-cm)	Normalized resistivity ($\mu\Omega$-cm)	$\Delta\rho$ ($\mu\Omega$-cm)
330	512.0	82.76	125.32	125.90	2.90
345	511.0	82.76	125.10	125.88	2.88
358	512.5	82.85	125.29	125.96	2.96
369	512.5	82.76	125.43	125.91	2.91
380	513.0	82.76	125.55	125.95	2.95
398	514.0	82.85	125.71	125.99	2.99
414	514.0	82.76	125.85	125.96	2.96
430	515.5	82.85	126.01	126.01	3.01
435	516.0	82.94	125.97	125.97	2.97
450	515.0	82.80	126.05	126.05	3.05
460	515.0	82.80	125.98	125.98	2.98
472	515.5	82.85	126.02	126.02	3.02
483	516.0	82.89	126.09	125.97	2.97
493	516.5	82.94	126.14	125.99	2.99
505	516.0	82.85	126.19	126.04	3.04
514	516.0	82.85	126.17	126.00	3.00
522	516.0	82.85	126.18	125.98	2.98
530	517.5	82.94	126.33	125.98	2.98
543	518.0	82.94	126.48	126.00	3.00
557	518.5	83.03	126.49	126.01	3.01
563	519.0	83.11	126.48	125.96	2.96
570	519.0	83.11	126.48	125.96	2.96
582	518.5	83.03	126.50	126.02	3.02
590	519.0	83.11	126.50	126.02	3.02
600	518.0	83.06	126.32	125.96	2.96
605	518.5	83.20	126.20	125.91	2.91
610	518.0	83.29	126.13	125.88	2.88
615	518.5	83.29	126.11	125.82	2.82
630	517.5	83.20	125.97	125.75	2.75
638	517.0	83.20	125.85	125.67	2.67
647	517.0	83.29	125.76	125.63	2.63
655	517.0	83.29	125.75	125.60	2.60
666	517.0	83.29	125.74	125.59	2.59
690	514.5	83.38	124.99	125.47	2.47
703	514.5	83.47	124.85	125.48	2.48
710	513.5	83.38	124.74	125.40	2.40
730	513.5	83.55	124.49	125.41	2.41
742	513.5	83.64	124.36	125.40	2.40
758	512.0	83.38	124.41	125.37	2.37

Table 6. (Continued)

Time (minutes)	Potential drop across specimen (μV)	Current (mA)	Resistivity ($\mu\Omega$-cm)	Normalized resistivity ($\mu\Omega$-cm)	$\Delta\rho$ ($\mu\Omega$-cm)
769	512.0	83.38	124.42	125.38	2.38
796	512.0	83.55	124.10	125.30	2.30
803	511.5	83.47	124.15	125.35	2.35
815	511.0	83.47	124.01	125.26	2.26
829	513.0	83.47	124.49	125.31	2.31
845	511.5	83.55	124.05	125.25	2.25
860	509.5	83.29	123.90	125.20	2.20
875	511.5	83.47	124.14	125.27	2.27
888	511.0	83.47	124.04	125.24	2.24
903	512.5	83.55	124.22	125.23	2.23
920	512.5	83.55	124.25	125.18	2.18
928	512.5	83.47	124.40	125.28	2.28
938	512.5	83.47	124.36	125.18	2.18
953	513.5	83.47	124.58	125.25	2.25
968	514.5	83.64	124.60	125.22	2.22
983	514.5	83.47	124.84	125.22	2.22
992	515.5	83.64	124.85	125.20	2.20
1013	516.5	83.73	124.98	125.22	2.22
1022	517.5	83.73	125.19	125.19	2.19
1042	519.0	83.64	125.67	125.19	2.19
1050	519.0	83.64	125.69	125.21	2.21
1100	570.5	83.47	138.43	124.95	1.95
1103	570.0	83.47	138.29	124.85	1.85
1106	570.5	83.55	138.32	124.64	1.64
1114	570.0	83.47	138.31	124.46	1.46
1121	570.0	83.47	138.32	124.40	1.40
1125	569.0	83.47	138.13	124.30	1.30
1132	568.0	83.47	137.83	124.22	1.22
1144	567.5	83.47	137.73	124.10	1.10
1152	567.5	83.47	137.76	124.13	1.13
1160	568.5	83.55	137.82	124.06	1.06
1175	568.0	83.55	137.70	123.99	0.99
1184	567.5	83.47	137.72	123.98	0.98
1190	567.0	83.47	137.62	123.97	0.97
1196	567.0	83.47	137.61	123.93	0.93
1210	569.0	83.47	138.14	123.93	0.93
1219	570.5	83.55	138.28	123.88	0.88
1225	570.5	83.55	138.27	123.82	0.82

Table 6. (Continued)

Time (minutes)	Potential drop across specimen (μV)	Current (mA)	Resistivity ($\mu\Omega$-cm)	Normalized resistivity ($\mu\Omega$-cm)	$\Delta\rho$ ($\mu\Omega$-cm)
1237	568.5	83.47	137.96	123.90	0.90
1255	566.5	83.47	137.44	123.81	0.81
1267	567.5	83.64	137.48	123.85	0.85
1275	568.5	83.73	137.56	123.85	0.85
1285	567.0	83.64	137.32	123.80	0.80
1300	567.0	83.55	137.46	123.76	0.76
1312	568.0	83.64	137.58	123.83	0.83
1336	566.0	83.55	137.19	123.75	0.75
1350	566.0	83.55	137.21	123.77	0.77
1359	566.0	83.55	137.26	123.82	0.82
1367	566.5	83.64	137.19	123.75	0.75
1386	567.5	83.64	137.43	123.77	0.77
1397	568.5	83.64	137.64	123.82	0.82
1416	568.0	83.73	137.45	123.77	0.77
1435	568.5	83.82	137.43	123.80	0.80
1448	568.5	83.82	137.43	123.80	0.80
1465	569.5	83.99	137.37	123.73	0.73
1484	568.5	83.82	137.35	123.82	0.82
1500	568.5	83.90	137.27	123.83	0.83
1525	569.5	83.82	137.63	123.75	0.75
1548	568.0	83.82	137.31	123.77	0.77

Table 7. Electrical resistivity data for specimen F ($\frac{\text{Area of cross-section}}{\text{Length}}$ = 0.0358203 cm)

Time (minutes)	Potential drop across specimen (μ V)	Current (mA)	Resistivity ($\mu\Omega$-cm)	Normalized resistivity ($\mu\Omega$-cm)	$\Delta\rho$ ($\mu\Omega$-cm)
0	275.0	81.36	121.05	118.05	0
3	275.5	81.36	121.27	118.38	0.38
7	277.0	81.54	121.79	118.25	0.25
10	277.0	81.88	121.26	118.52	0.52
25	278.0	82.06	121.34	118.82	0.82
32	279.0	82.15	121.69	119.25	1.25
45	277.5	82.15	120.97	119.35	1.35
55	277.0	82.24	120.55	119.65	1.65
66	276.5	82.24	120.39	119.91	1.91
77	276.5	82.24	120.43	120.01	2.01
86	276.5	82.06	120.68	120.27	2.27
98	276.5	82.24	120.43	120.43	2.43
102	277.0	82.24	120.62	120.56	2.56
113	277.0	82.15	120.72	120.72	2.72
128	277.0	82.24	120.70	120.75	2.75
133	277.5	82.24	120.93	120.93	2.93
142	276.5	82.24	120.95	120.95	2.95
152	277.5	82.15	121.05	121.12	3.12
158	278.0	82.24	121.14	121.04	3.04
167	278.5	82.32	121.15	121.15	3.15
180	278.5	82.32	121.21	121.21	3.21
185	278.5	82.24	121.34	121.34	3.34
198	279.0	82.32	121.40	121.40	3.40
206	280.0	82.59	121.41	121.41	3.41
214	280.0	82.59	121.46	121.46	3.46
218	280.5	82.59	121.62	121.57	3.57
235	281.5	82.76	121.77	121.59	3.59
245	285.5	82.67	122.05	121.63	3.63
255	282.0	82.76	122.03	121.77	3.77
265	285.5	82.67	122.04	121.77	3.77
280	281.0	82.59	121.90	12..78	3.78
285	281.0	82.59	121.92	121.92	3.92
325	280.0	82.76	121.25	121.97	3.97
332	279.0	82.76	120.84	122.14	4.14
345	280.0	82.76	121.16	122.12	4.12
353	280.5	82.85	121.33	122.18	4.18
360	281.0	82.76	121.55	122.15	4.15

Table 7. (Continued)

Time (minutes)	Potential drop across specimen (μV)	Current (mA)	Resistivity ($\mu\Omega$-cm)	Normalized resistivity ($\mu\Omega$-cm)	$\Delta\rho$ ($\mu\Omega$-cm)
373	281.0	82.76	121.68	122.28	4.28
397	282.0	82.76	121.99	122.30	4.30
412	280.5	82.76	121.43	122.27	4.27
421	282.5	82.76	122.38	122.38	4.38
448	283.5	82.85	122.53	122.48	4.48
452	283.0	82.80	122.49	122.49	4.49
458	283.0	82.80	122.49	122.49	4.49
476	283.5	82.89	122.50	122.56	4.56
490	283.0	82.94	122.29	122.52	4.52
500	283.5	82.94	122.42	122.56	4.56
510	283.5	82.94	122.44	122.62	4.62
522	284.0	82.94	122.64	122.58	4.58
528	284.0	82.94	122.73	122.61	4.61
550	284.5	82.94	122.82	122.60	4.60
563	285.0	83.11	122.85	122.67	4.67
570	285.0	83.11	122.90	122.66	4.66
582	285.5	83.03	123.21	122.66	4.66
593	286.0	83.11	123.27	122.67	4.67
604	285.5	83.11	123.10	122.62	4.62
610	285.5	83.29	122.81	122.51	4.51
620	285.5	83.29	122.80	122.50	4.50
633	285.0	83.20	122.64	122.40	4.40
640	285.5	83.29	122.70	122.46	4.46
665	284.0	83.20	122.31	122.26	4.26
675	284.5	83.29	122.36	122.30	4.30
690	284.0	83.38	121.96	122.26	4.26
704	283.5	83.47	121.67	122.15	4.15
709	283.5	83.47	121.64	122.18	4.18
735	283.5	83.64	121.37	122.15	4.15
754	282.5	83.47	121.31	122.15	4.15
759	282.5	83.47	121.23	122.07	4.07
770	282.5	83.47	121.30	122.11	4.11
775	282.5	83.47	121.23	122.05	4.05
781	283.0	83.55	121.20	122.10	4.10
790	282.5	83.55	121.09	122.10	4.10
800	282.0	83.47	120.96	122.04	4.04
810	281.5	83.38	121.02	122.10	4.10
815	282.0	83.47	121.09	122.05	4.05
826	282.5	83.47	121.23	122.01	4.01

Table 7. (Continued)

Time (minutes)	Potential drop across specimen (μV)	Current (mA)	Resistivity ($\mu\Omega$-cm)	Normalized resistivity ($\mu\Omega$-cm)	$\Delta\rho$ ($\mu\Omega$-cm)
836	282.0	83.38	121.20	121.98	3.98
850	281.5	83.38	120.98	122.06	4.06
865	281.5	83.47	129.83	122.03	4.03
870	281.5	83.47	120.88	122.08	4.08
890	281.5	83.47	120.84	122.04	4.04
920	280.0	83.47	120.15	121.99	3.99
930	283.0	83.55	121.26	122.04	4.04
940	282.5	83.55	121.19	121.97	3.97
955	283.0	83.55	121.31	121.97	3.97
966	283.5	83.64	121.35	121.95	3.95
990	284.0	83.64	121.55	122.03	4.03
995	284.0	83.64	121.57	121.95	3.95
1020	284.5	83.64	121.90	121.95	3.95
1030	285.5	83.64	122.29	121.99	3.99
1040	285.5	83.55	122.43	121.95	3.95
1101	322.0	83.47	138.20	121.40	3.40
1109	321.5	83.55	137.91	120.90	2.90
1111	321.0	83.47	137.81	120.75	2.75
1120	321.5	83.47	137.93	120.53	2.53
1127	320.5	83.47	137.62	120.40	2.40
1143	320.0	83.47	137.15	120.18	2.18
1152	319.5	83.47	137.11	120.01	2.01
1160	319.5	83.55	137.01	119.92	1.92
1175	319.5	83.47	137.12	119.90	1.90
1180	319.0	83.47	136.98	119.82	1.82
1196	319.0	83.47	136.85	119.75	1.75
1206	319.0	83.47	136.86	119.64	1.64
1215	318.5	83.47	136.66	119.65	1.65
1225	318.5	83.47	136.70	119.58	1.58
1234	318.5	83.47	136.60	119.62	1.62
1240	319.0	83.47	136.95	119.54	1.54
1248	319.0	83.47	136.82	119.54	1.54
1265	318.5	83.55	136.52	119.48	1.48
1275	318.5	83.64	136.43	119.51	1.51
1286	318.5	83.64	136.39	119.47	1.47
1297	318.0	83.47	136.51	119.43	1.43
1305	318.5	83.47	136.63	119.48	1.48
1314	317.5	83.47	136.33	119.43	1.43
1330	318.5	83.55	136.61	119.43	1.43

Table 7. (Continued)

Time (minutes)	Potential drop across specimen (μV)	Current (mA)	Resistivity ($\mu\Omega$-cm)	Normalized resistivity ($\mu\Omega$-cm)	$\Delta\rho$ ($\mu\Omega$-cm)
1339	319.0	83.55	136.70	119.48	1.48
1352	319.0	83.55	136.68	119.46	1.46
1370	318.0	83.55	136.31	119.45	1.45
1380	318.5	83.55	136.56	119.40	1.40
1387	319.0	83.64	136.62	119.46	1.46
1396	319.0	83.64	136.69	119.41	1.41
1409	319.0	83.64	136.50	119.43	1.43
1419	319.0	83.73	136.56	119.46	1.46
1426	319.0	83.73	136.56	119.43	1.43
1440	319.0	83.73	136.49	119.45	1.45
1465	320.0	83.99	136.55	119.45	1.45
1475	319.5	83.82	136.49	119.39	1.39
1495	319.5	83.90	136.39	119.39	1.39
1512	319.5	83.90	136.43	119.39	1.39
1522	319.5	83.73	136.74	119.44	1.44
1530	319.0	83.64	136.55	119.39	1.39
1542	319.5	83.82	136.32	119.40	1.40

Table 8. Electrical resistivity data for gamma irradiation ($\frac{\text{Area of cross-section}}{\text{Length}}$ = 0.03144815 cm)

Time (hours)	Potential drop across specimen (μV)	Current (mA)	Resistivity ($\mu\Omega$-cm)	Normalized resistivity at 80°F ($\mu\Omega$-cm)
0	494.5	121.24	128.29	127.89
1.00	493.0	120.37	128.77	127.87
1.50	494.0	120.77	128.68	127.76
3.75	496.5	121.37	128.68	127.82
6.58	499.5	122.12	128.67	127.84
9.21	502.0	122.83	128.54	127.93
11.23	501.5	122.48	128.81	127.97
12.92	501.0	122.12	129.01	127.96
22.43	501.5	122.12	129.18	128.07
24.73	502.0	122.48	128.98	128.02
27.78	493.5	120.37	128.93	127.94
35.70	494.5	120.77	128.74	127.83
48.50	499.0	122.00	128.79	127.84
52.17	497.5	121.57	128.68	127.58
59.50	502.0	122.74	128.72	127.63
70.00	501.5	122.28	128.96	127.81
75.25	504.0	122.86	129.03	127.98
82.78	503.5	122.70	129.08	128.01
97.27	502.0	122.38	129.05	128.08
118.5	500.5	121.99	129.06	128.04
142.0	499.5	121.79	128.97	128.05

Figure 16. Resistivity of the unirradiated samples against current

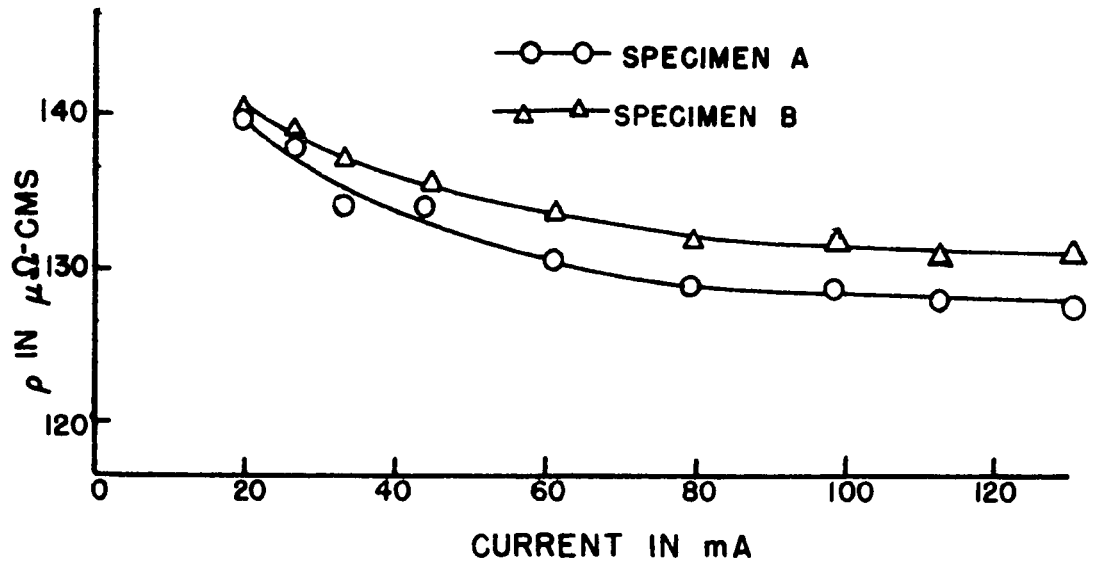
SPECIMEN A
SPECIMEN B
140
130
120
ρ IN μΩ-CMS
0
20
40
60
80
100
120
CURRENT IN mA

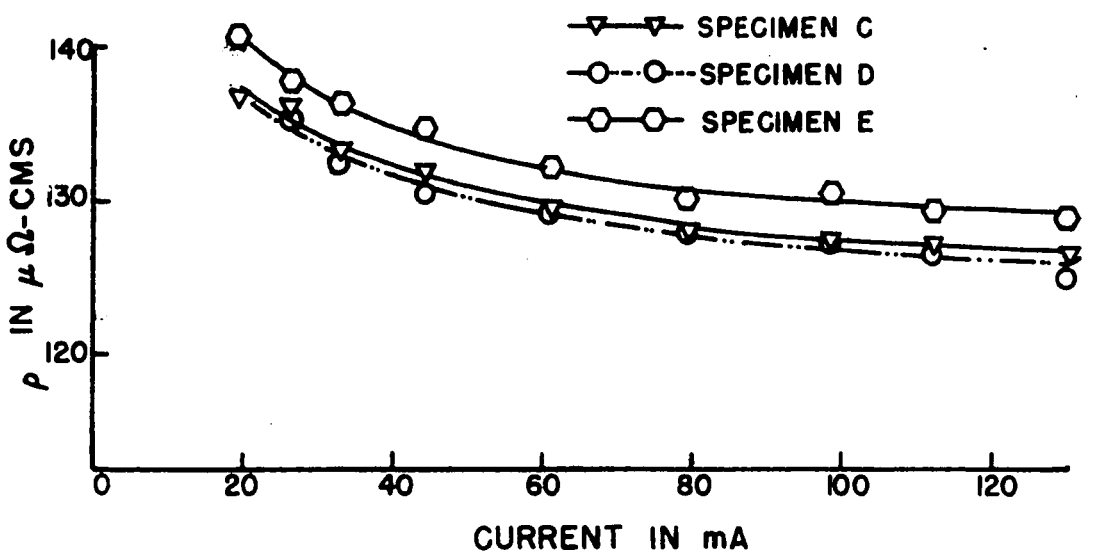
SPECIMEN C
SPECIMEN D
SPECIMEN E
140
130
120
ρ IN μΩ-CMS
0
20
40
60
80
100
120
CURRENT IN mA

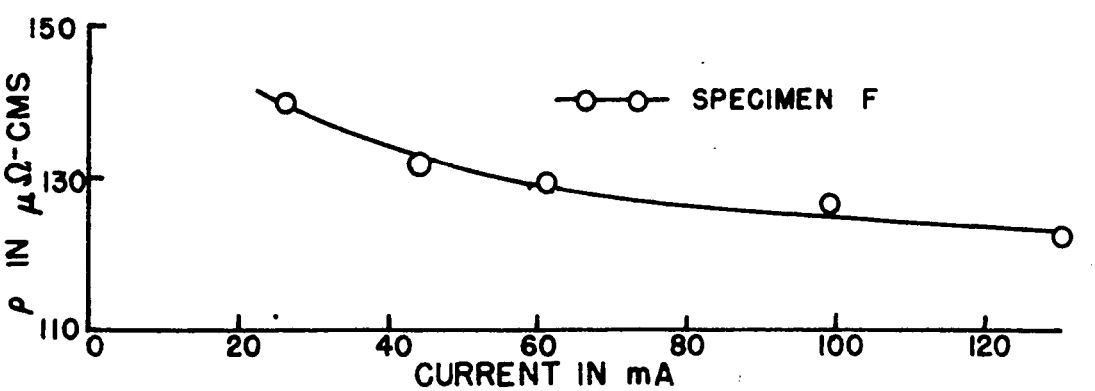
SPECIMEN F
150
130
110
ρ IN μΩ-CMS
0
20
40
60
80
100
120
CURRENT IN mA

Figure 17. Resistivity of the unirradiated specimens against temperature

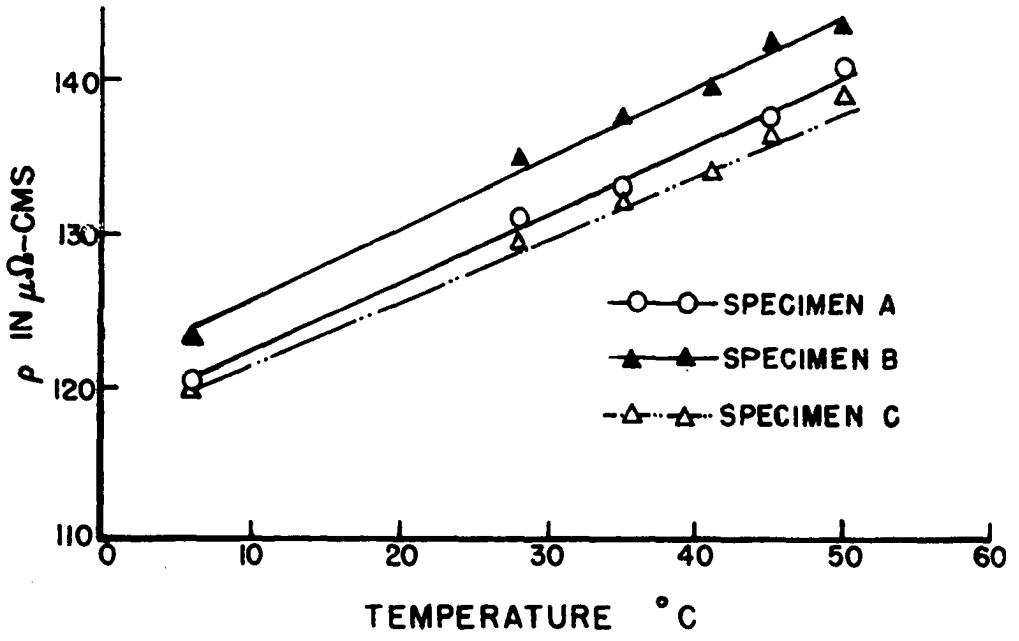
140
130
120
110
ρ IN μΩ-CMS
0
10
20
30
40
50
60
TEMPERATURE °C
SPECIMEN A
SPECIMEN B
SPECIMEN C

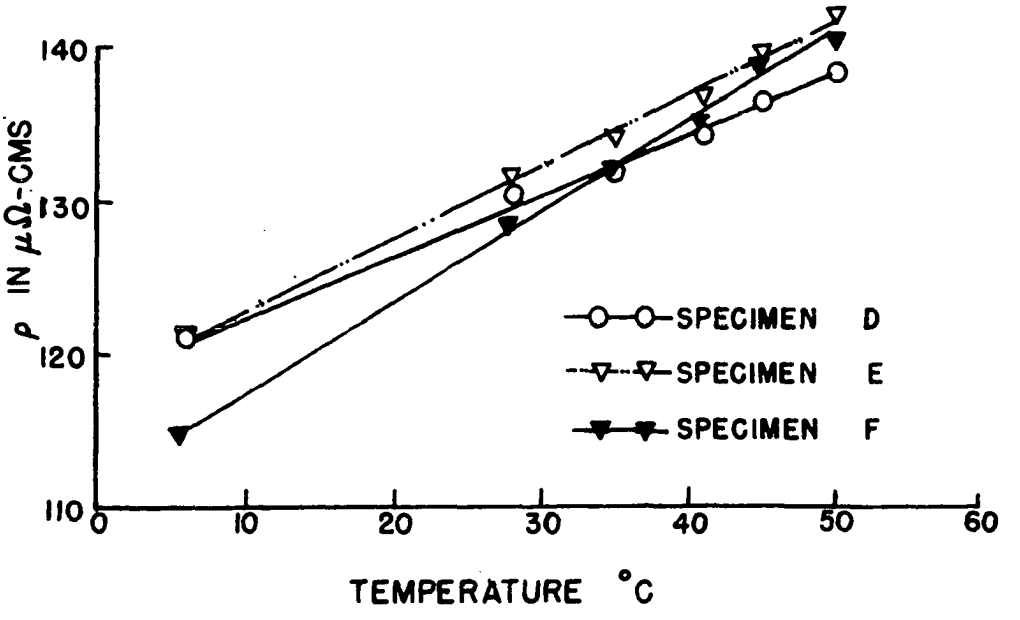
140
130
120
110
ρ IN μΩ-CMS
0
10
20
30
40
50
60
TEMPERATURE °C
SPECIMEN D
SPECIMEN E
SPECIMEN F